



16 **Abstract**

17 Thermal responses of inland waters to climate change varies on global and regional scales. The extent of warming
18 is determined by system-specific characteristics such as fluvial input. Here we examine the impact of ongoing
19 climate change on two alpine tributaries, the Aare River and Rhône River, and their respective downstream, peri-
20 alpine lakes: Lake Biel and Lake Geneva. We propagate regional atmospheric temperature effects into river
21 discharge projections. These, together with anthropogenic heat sources, are in turn incorporated into simple and
22 efficient deterministic models that predict future water temperatures, river-borne suspended sediment
23 concentration (SSC), lake stratification and river intrusion depth/volume into the lakes. Climate-induced shifts in
24 river discharge regimes, including seasonal flow variations, act as positive and negative feedbacks in influencing
25 river water temperature and SSC. Discharge-dependent increase of river temperature in turn results in large
26 seasonal shifts in warming of downstream lakes. Their hydraulic residence times control seasonal variations in
27 climate-induced heating. Previous studies suggest that climate change will diminish deep-water oxygen renewal
28 in lakes. We find that climate-related seasonal variations in river temperatures and SSC affect the rate of deep-
29 penetrating river intrusions. Seasonal variations (with decreasing flows in summer and increasing flows in winter)
30 determine water input reaching the deepest parts of lakes. The river-lake model results described here show an
31 annual increase in deep-water renewal. This process may therefore counteract otherwise negative effects of
32 climate change on deep-water oxygen supply in lakes. Our findings provide a template for evaluating the response
33 of similar hydrologic systems to on-going climate change.

34

35 **Copyright statement**

36 All material in this manuscript has been produced by the authors themselves, nothing is republished.



37 **1 Introduction**

38 The thermal and hydrodynamic responses of lakes to climate change are considerably diverse. Observed responses
39 vary on global, regional and even local scales (O'Reilly et al., 2015). Even neighbouring freshwater bodies can
40 react differently to a given increase in air temperature. This indicates that lake-specific characteristics will
41 determine the response to climate change (for clarity and brevity, we refer to anthropogenic climate change simply
42 as 'climate change' or 'climate' from now on). Local factors which affect climate warming of lakes include,
43 among others, morphology (Toffolon et al., 2014), irradiance absorption (Kirillin, 2010; Williamson et al., 2015),
44 local weather conditions (Zhong et al., 2016), stratification (Piccolroaz et al., 2015), atmospheric brightening
45 (Fink et al., 2014a) and ice cover (Austin and Colman, 2007).

46 Throughflows affect epilimnion and hypolimnion temperatures of lakes. Studies of climate impact typically do
47 not address these sorts of subtleties in lake dynamics due to lack of data or difficulties in predicting future
48 temperature and discharge conditions (Fenocchi et al., 2017). Several studies of large lakes suggest that major
49 tributaries play only a minor role in climate-induced warming and deep-water oxygen renewal (Fink et al., 2014a;
50 Schwefel et al., 2016). Medium- and smaller-scale lakes are, however, more abundant than large lakes (Downing
51 et al., 2006) and exhibit a greater degree of sensitivity to point sources of anthropogenic thermal input which can
52 affect temperature and stratification (Kirillin et al., 2013; Råman Vinnå et al., 2017). Medium- and small-sized
53 lakes also make a more significant contribution to the temperature-dependent global greenhouse gas budget
54 (Holgerson and Raymond, 2016). Accurate prediction of climate change impact therefore requires a more detailed
55 understanding of small- to medium-scale lake and tributary systems.

56 Climate change exerts dual influence on alpine rivers by introducing variation to both flow and temperatures.
57 Discharge variation takes the form of less flow in summer and more flow in winter due to warmer high altitude
58 snow and ice melt/runoff regimes (Addor et al., 2014; Birsan et al., 2005) which also influence river temperature
59 (Isaak et al., 2012; Van Vliet et al., 2013). Increased air temperature may also enhance erosion rates in river basins
60 thereby supplementing river-borne suspended sediment loads (Bennett et al., 2013). River temperature and
61 suspended sediment content determine water density and by extension, the depth of river plume intrusions into
62 downstream lakes or reservoirs. The depth and volume of river intrusion plumes determine deep-water oxygen
63 renewal, especially for deeper lakes where climate-related warming can reduced seasonal deep convective mixing
64 and thereby deplete deep-water oxygen (Schwefel et al., 2016). Major (deeply penetrating) river intrusion events
65 typically occur due to flooding, which introduces large sediment loads into the river (Fink et al., 2016). The
66 frequency and volume of floods in the Alps are notoriously hard to predict, although a decrease in floods has
67 occurred in association with recent warmer summers observed in the Alps (CH2011, 2011; Glur et al., 2013).

68 Recent model studies have identified inland waters as risk-hotspots under expected climate change scenarios
69 (Pachauri et al., 2015). These systems require a more detailed analysis given their role in supporting fisheries,
70 agriculture, drinking water production, heat extraction/release and hydropower. This paper examines complex
71 interactions between tributaries and lakes in response to temperature increases and other modifications expected
72 from climate change. Our objectives were to quantify the impact of specific climate change scenarios on (i) alpine
73 tributaries and (ii) downstream peri-alpine lakes with a focus on river-borne suspended sediment concentration
74 (SSC), water temperature, stratification and river intrusion depth and volume.



75 Our analysis used coupled river-lake models to build on previous research by Fink et al. (2016). These authors
76 investigated the effect of flood frequencies on deep-water renewal under established climate change scenarios.
77 Their work did not generate tightly constrained estimates for flooding events. Our analysis therefore provisionally
78 assumed that flood frequency does not change in the future. In addition to these sources of natural variation, our
79 models addressed variation in river discharge regimes (i.e. daily mean level shift) under the specified A1B climate
80 change scenario. These in turn affect SSC and thermal regimes for rivers and their associated downstream lakes.
81 Our analysis furthermore shows that local point sources of anthropogenic thermal pollution can have major impact
82 on the response of inland waters to climate change as previously suggested by Fink et al. (2014b).

83

84 **2 Methods**

85 **2.1 Approach**

86 Investigation of tributary-influence on lake response to climate change followed these procedural steps:

- 87 (i) Define river temperature and SSC models for two major alpine rivers and designate a one-
88 dimensional lake model for a large- and a medium-sized peri-alpine lake.
- 89 (ii) Integrate model (i) with a state-of-the-art river intrusion scheme. Figure 1 shows integration of one-
90 way component models.
- 91 (iii) Obtain and apply estimates of future regional air temperature, tributary discharge and changes in
92 local anthropogenic thermal emissions to both river and lake models.
- 93 (iv) Identify patterns in model outputs of water temperature, SSC, lake stratification and river intrusion
94 parameters (volume and depth).

95

96 **2.2 Study area**

97 This study examined two warm, monomictic, freshwater peri-alpine lakes in western Switzerland, Lake Biel (LB;
98 7°10' E, 47°5' N) and Lake Geneva (LG; 6°31' E, 46°27' N). Large tributaries originating in the Alps, the Aare
99 River and Rhône River, feed into LB and LG, respectively (Fig. 2).

100 LG is a large, meso-eutrophic lake resting at 372 m elevation and covering an area of 580 km². It reaches a
101 maximum depth of 309 m and holds a volume of 89 km³ with an average hydraulic residence time of 11.5 years.
102 Complete seasonal deep convective mixing only occurs on average every fifth winter but is predicted to become
103 less frequent with on-going climate change (Perroud and Goyette, 2010; Schwefel et al., 2016). The average
104 surface water temperature has increased by ~0.11° C decade⁻¹ to ~0.52° C decade⁻¹ (Gillet and QueTin, 2006;
105 O'Reilly et al., 2015). The Rhône River supplies ~75% of LG's inflow and experienced a temperature increase of
106 ~0.21 °C decade⁻¹ from 1978 to 2002 (Hari et al., 2006).

107 LB is a 74 m deep, meso-eutrophic, medium-sized lake resting at an elevation of 429 m. It covers a surface area
108 of 39.3 km² and holds a volume of 1.18 km³ with hydraulic residence time of 58 days. Complete deep convective
109 mixing occurs every winter and effectively replenishes the oxygen-depleted deep-water. The Aare River provides
110 ~61% of LB's inflow and experienced a 0.34 °C decade⁻¹ increase in temperature from 1978 to 2002 (Hari et al.,



111 2006). Several dams/lakes trap sediment along the upstream Aare course and influence flow in ways that increase
 112 sediment settling and water temperature prior to entering LB. The Mühleberg Nuclear Power Plant (MNPP),
 113 situated ~19 km upstream from LB (7°16' E, 46°59' N; Fig. 2) represents a point-source of thermal pollution.
 114 Planned for decommission in 2019, the plant emits 700 MW of heat into Aare and substantially warms the river
 115 water (Råman Vinnå et al., 2017). The ~8 km long Zihlkanal, LB's second largest tributary, supplies ~32% of the
 116 lake inflow and connects LB to Lake Neuchâtel (Fig. 2). This tributary is neglected here since it mainly transport
 117 lake surface water, which has approximately the same temperature as LB surface water and thus heats equally.

118

119 2.3 River models

120 2.3.1 Temperature

121 Uncertainty concerning river morphology, heat fluxes, shadowing and atmospheric conditions such as wind speed
 122 and cloudiness (Caissie, 2006) pose a significant challenge to accurate modelling of future river temperatures.
 123 Deterministic models typically require detailed knowledge unavailable for future climate scenarios. Regressions
 124 and stochastic models rely heavily on observed natural variability applicable to a given time frame and typically
 125 do not include inputs representing additional or interacting physical processes. On their own, these sorts of “black
 126 box” models cannot balance trade-offs between constraints available from empirical data and the complexity
 127 offered by theoretical frameworks.

128 To overcome these limitations, we used the hybrid model air2stream (Toffolon and Piccolroaz, 2015). The model
 129 combines the simplicity of stochastic models with accurate representation of the relevant physical processes
 130 affecting temperature. Similar to the neural networks approach, the model calculates river water temperature (T_w)
 131 through a Monte Carlo-like calibration process, which identifies optimal parameters for weighting physically
 132 dependent variables. We used the eight-parameters (a_1 to a_8) version of the model which incorporates air
 133 temperature (T_a) and river discharge (Q) as a function of time (t).

$$134 \quad \frac{dT_w}{dt} = \frac{1}{\delta} \left\{ a_1 + a_2 T_a(t) - a_3 T_w(t) + \theta \left[a_5 + a_6 \cos \left(2\pi \left(\frac{t}{t_y} - a_7 \right) \right) - a_8 T_w(t) \right] \right\}; \quad (1)$$

$$\delta = \theta^{a_4}; \theta = Q(t)/\bar{Q};$$

135 where t is expressed in years and t_y represents one year. Both Aare and Rhône (stations 2085 and 2009,
 136 respectively, Fig. 2) provided calibration (1990 – 1999) and validation data (2000 - 2009). Table 1 and Fig. 3
 137 show best-fit parameters and model performance statistics. Model sensitivity to variation in T_w was assessed by
 138 removing MNPP thermal pollution and repeating the calibration/validation for station 2085 (Table 1).

139

140 2.3.2 Suspended sediment concentration

141 Water density and intrusion depth of river water into downstream lakes is influenced by SSC. Intensive flow
 142 events create high levels of SSCs (Rimmer and Hartmann, 2014), as can exposure/erosion of sediment sources



143 within the river basin through the so-called hysteresis effect, in which SSC varies for the same level of discharge
144 (Tananaev, 2012). River discharge regimes have been predicted to change in the future (Birsan et al., 2005),
145 suggesting that SSCs will also change. To simulate future SSCs, we used the supply-based rating model described
146 in Doomen et al. (2008), which Fink et al. (2016) adapted to the Rhine River.

147 The model consists of a base level SSC (g m^{-3}) function expanded to express erosion of sediment at high discharge
148 and sediment accumulation at low discharge. The model is expressed as

$$149 \quad SSC(t) = m + b_1 Q(t)^{c_1} + d_1 d_2 b_2 (Q(t) - Q_{th})^{c_2} - b_3 (1 - d_2), \quad (2)$$

150 where b_x , c_x and m are adjustable parameters in combination with the threshold discharge (Q_{th}), which determines
151 whether erosion or deposition occurs within the river. The parameters d_1 and d_2 control the deposition/erosion
152 of/from the river sediment storage (ψ (g))

$$153 \quad d_1 = \begin{cases} 0: \psi = 0 \\ 1: \psi > 0 \end{cases} \quad (3)$$

$$154 \quad d_2 = \begin{cases} 0: Q \leq Q_{th} \\ 1: Q > Q_{th} \end{cases} \quad (4)$$

155 Erosion occurs if Q exceeds Q_{th} and the river basin contains erodible sediment ($\psi > 0$). Sedimentation occurs if Q
156 is smaller than Q_{th} . The change in ψ over time can be formulated as

$$157 \quad \frac{d\psi}{dt} = \left(b_3 (1 - d_2) - d_1 d_2 b_2 (Q(t) - Q_{th})^{c_2} \right) Q(t) \quad (5)$$

158 Parameters in equations (2) to (5) were calibrated (2013) and validated (2014) through a evolutionary algorithm
159 (Fink et al., 2016). Table 2 and Fig. 4 give model performance statistics and best-fit parameter values.

160

161 **2.4 Lake model**

162 We used the one-dimensional model SIMSTRAT (Goudsmit et al., 2002) to assess the impact of climate change
163 on temperature and deep-water renewal in LB and LG. The model calculates heat fluxes and vertical mixing driven
164 by wind and the internal wave field. SIMSTRAT has been adapted to and validated for multiple lakes including
165 Lake Zürich (Peeters et al., 2002), LG (Perroud and Goyette, 2010; Schwefel et al., 2016), Lake Neuchâtel
166 (Gaudard et al., 2016), Lake Constance (Fink et al., 2014b; Wahl and Peeters, 2014) and LB (Răman Vinnă et al.,
167 2017). Here we used best-fit parameters already established and validated by Schwefel et al. (2016) for LG and
168 by Răman Vinnă et al. (2017) for LB (Table 3).

169 Building upon the model developed by Răman Vinnă et al. (2017), we introduced an extended river intrusion
170 scheme described in Appendix A1 (including sensitivity analysis). Lake water entrainment into plunging
171 underflows are modelled as proposed by Akiyama and Heinz (1984) with additional sedimentation of suspended
172 load (Mulder et al., 1998; Syvitski and Lewis, 1992). The method addresses the transition of a homogenous open



173 channel flow to a stratified underflow where entrainment and settling of sediment depend on bottom slope angle.
174 The model scheme consists of (i) the homogenous region where river water makes up the entire water column,
175 (ii) the plunging region where the plume separates from the lake surface and (iii) the underflow region where the
176 plume descends downslope while entraining surrounding water until it separates from the bottom and intrudes
177 into the lake interior (Fink et al., 2016).

178

179 **2.5 Data, hydrology and climate forcing**

180 The models described above used hourly resolved data from 1989 to 2009 as inputs. For calibration/validation of
181 river temperature, we used flow and temperature data from the Aare monitoring station #2085 (Fig. 2; 7°11' E,
182 47°3' N) and from the Rhône monitoring station #2009 (Fig. 2; 6°53' E, 46°21' N). The nearest meteorological
183 stations, Mühleberg (#5530 Fig. 2; 7°17' E, 46°58' N) for Aare and Aigle (#7970 Fig. 2; 6°55' E, 46°20' N) for
184 Rhône, provided air temperature data. Due to insufficient representation of high turbidity events, we
185 calibrated/validated the SSC model with turbidity data converted to SSC with suspended load mass samples from
186 2013 and 2014.

187 The meteorological data used for SIMSTRAT included air temperature, vapour pressure, wind speed, solar
188 radiation and cloud cover. These data were collected from the meteorological stations Cressier (#6354 Fig. 2;
189 7°03' E, 47°03' N) for LB and Pully (#8100 Fig. 2; 6°40' E, 46°31' N) for LG. Râman Vinnâ et al. (2017) and
190 Schwefel et al. (2016) provide additional information on climate data inputs to the one-dimensional model. The
191 model's river intrusion scheme requires as input the slope angle travelled by the river underflow, which was
192 obtained from a 25 m resolved digital height model (DHM25). Vertical temperature profiles, sampled at the
193 deepest location of both lakes in January 1989, were used as initial conditions.

194 Van Vliet et al. (2013) suggested that river discharge and air temperature should be used while predicting future
195 river temperatures. We incorporated recent findings of climate-induced changes in air temperature and river
196 discharge regimes to model both future river temperature and sediment loads. Seasonal mean predictions for air
197 temperature increase in western Switzerland (Fig. 2), were estimated from CH2011 (2011) under the A1B
198 emission scenario (balanced use of renewable and fossil fuels) using results from twenty regional climate models.
199 Flow projections were obtained from published results generated by the PREVAH (PREcipitation-Runoff-
200 EVApotranspiration HRU Model) hydrological model (Viviroli et al., 2009) using a gridded configuration as
201 described in Speich et al. (2015) and Kobierska et al. (2011). The model explicitly incorporates changes in glacial
202 extent, snow melt, catchment runoff, floods and low water flows (FOEN, 2012; Bosshard et al., 2013; Speich et
203 al., 2015). The PREVAH outcomes for the 1981-2009 period have been validated with data from 65 river gauges
204 (Speich et al., 2015), including the two gauges upstream of LG (Rhône, #2009 in Fig. 2) and LB (Aare, #2085 in
205 Fig. 2) used here.

206

207 **2.6 Model scenarios**

208 Six different model scenarios were used to propagate climate change effects through the major tributaries and
209 their associated downstream lakes. Model scenarios LG1 to LG3 represented LG while LB1 to LB3 represented



210 LB (Table 4). Each scenario includes three time periods: a reference period (1990-2009), a near-future period
211 (2030-2049) and a far-future period (2080-2099). The twenty-year intervals allowed us to resolve natural
212 variations at seasonal and shorter time scales. We initialized the models one year prior to the investigated period
213 for each time frame (1989, 2029 and 2079) in order to remove effects of initial conditions.

214 Scenarios LG1 and LB1 excluded river inflow in order to isolate lake response to climate change from potential
215 tributary influence. Scenarios LG2, LG3, LB2 and LB3 were used to differentiate between the effects of tributary
216 temperature and SSC, and to provide model sensitivity estimates. The LB3 scenario excluded MNPP thermal
217 pollution from near-future and far-future time periods but not from the reference period. The LB2 scenario
218 included thermal pollution in modelling river water temperature. Scenarios LB2, LB3 and LG3 included SSC
219 while LG2 did not. Low SSC values found in the Aare data resulted in negligible differences between models
220 including and excluding SSC. Because they served primarily validation and sensitivity analysis purposes, the
221 Aare/LB model results excluding particles and including/excluding MNPP thermal pollution (LB4 and LB5) are
222 relegated to Appendix Figure B1 and not discussed further. Scenarios LG3 and LB3 represent expected future
223 developments.

224 The unmodified air temperature and modelled river discharge/temperature/SSC were used as inputs for the
225 reference periods. Near-future and far-future models incorporated predicted changes in air temperature and river
226 discharge/temperature/SSC with maximum, medium/mean and minimum values serving as envelopes for each
227 parameter (Figs. 2a and 5). This strategy gave nine simulations (three for scenario LG1 and LB1 which exclude
228 rivers, i.e. no variation of discharge nor river temperature) for each near-future and far-future time period.
229 Predicted results included a total of 87 model runs. Upper, mean and lower impact estimates (described and
230 interpreted below) were derived from the nine basic model runs.

231

232 **3 Results**

233 **3.1 Rivers**

234 The seasonality of predicted river discharge (Q) from FOEN (2012) varies with respect to the reference period
235 1990-2009 (Figs. 5a and 5b). The PREVAH model show a future decrease of mean summer discharge (1st April
236 to 30th September) for both the Aare ($-3.7 \text{ m}^3 \text{ s}^{-1} \text{ decade}^{-1}$, #2085) and Rhône ($-3.8 \text{ m}^3 \text{ s}^{-1} \text{ decade}^{-1}$, #2009). The
237 decrease in summer will be compensated by an observed increase in winter flow (1st October to 31st March) of the
238 Aare ($+3.3 \text{ m}^3 \text{ s}^{-1} \text{ decade}^{-1}$) and Rhône ($+3.7 \text{ m}^3 \text{ s}^{-1} \text{ decade}^{-1}$). These results confirm previous findings presented
239 in Addor et al. (2014) and Bosshard et al. (2013).

240 Regional air temperatures from the A1B emission scenario ($\sim +0.32 \text{ }^\circ\text{C decade}^{-1}$; CH2011, 2011; Fig. 2a) cause a
241 predicted increase in mean annual water temperature (T) for both the Aare ($\sim +0.10 \text{ }^\circ\text{C decade}^{-1}$) and the Rhône
242 ($\sim +0.08 \text{ }^\circ\text{C decade}^{-1}$). Both rivers experience seasonal variations in temperature increase similar to that predicted
243 for air temperatures (Figs. 2a, 5e and 5f). The effect is strongest in Aare during summer with warming of up to
244 $+2.5 \text{ }^\circ\text{C}$ in water temperatures for the far-future time period relative to the reference period.

245 Thermal pollution from MNPP in the Aare during the reference period (blue-green line in Fig. 5e, Råman Vinnå
246 et al., 2017) causes approximately twice as much heating in winter relative to warming from climate change in



247 the far-future. In summer, the relationship reverses with minor MNPP warming relative to that induced by climate
248 change. The net effect of climate warming and MNPP decommission (i.e. removal of MNPP heat from near-future
249 and far-future time periods) on the Aare is cooling in winter and warming in summer relative to the reference
250 period (Fig. 5c). Climate change and local anthropogenic thermal input can thus exert similar impacts on river
251 temperatures, consistent with previous findings by Wright et al. (1999).

252 Like river temperatures, SSCs depend on river discharge. Our model therefore show SSC increasing in winter and
253 decreasing in summer due to shifts in discharge regime (Figs. 5g and 5h). The model results for Rhône exhibit a
254 mean seasonal increase of $+14 \text{ g m}^{-3} \text{ decade}^{-1}$ in winter and a decrease of $-11 \text{ g m}^{-3} \text{ decade}^{-1}$ in summer. For reasons
255 explained above (section 2.2), results for the Aare show less variation, with a seasonal increase of $+0.3 \text{ g m}^{-3}$
256 decade^{-1} in winter and a decrease of $-0.4 \text{ g m}^{-3} \text{ decade}^{-1}$ in summer. Altered temperature and SSC caused increases
257 and decreases in water density for both rivers in winter and summer, respectively.

258

259 3.2 Lakes

260 Warmer air temperatures (Fig. 2a) predicted from climate change resulted in temperature increases in both LG
261 and LB for all scenarios (Table 5). Models showed the highest warming rates in the epilimnion, intermediate
262 values throughout the metalimnion and the lowest rates in the hypolimnion (Table 5). We defined the epilimnion,
263 metalimnion and hypolimnion using the water column stability method described in Råman Vinnå et al. (2017).
264 The predicted warming of LG varied only slightly among the three-different scenarios (Figs. 6a to 6c). Predicted
265 warming of LB depend strongly on the scenario used (Figs. 6d to 6f).

266 Similar to the predicted warming patterns for rivers (section 3.1), both lakes showed seasonally varying warming
267 patterns. Reduced warming corresponds with periods of high river discharge (Figs. 5a and 5b). This cooling effect
268 occurs primarily in winter and mid-summer, focussed in depth to the level of river intrusion (Figs. D1b, D1d and
269 7c to 7f). Model results showed a greater degree of fluctuations of the warming in LB than in LG. This probably
270 results from the greater influence of the Aare on LB compared to that of the Rhône on LG, as LG has a longer
271 hydraulic residence time. Scenario LB1, which excludes river intrusion, showed only limited seasonal variation
272 in warming (Figs. C1c and C1e). According to these results, the closure of MNPP could offset climate-induced
273 warming of LB by $\sim 25\%$ ($\sim -0.02 \text{ }^\circ\text{C decade}^{-1}$).

274 Model results show that enhanced warming of the epilimnion relative to the hypolimnion strengthens stratification
275 (Figs. 7g and 7h). This enhances the duration of stratification (for both lakes $\sim +2 \text{ days decade}^{-1}$; Table 5) and
276 slightly elevates the thermocline (in LB $\sim -0.1 \text{ m decade}^{-1}$ and in LG $\sim -0.05 \text{ m decade}^{-1}$; Table 5). We used the
277 Schmidt (1928) stability (S) equation to estimate stratification strength (J m^{-2}):

$$278 \quad S = \frac{g}{A_0} \sum_{z=0}^{z_{\max}} (z - z_m) (\rho(z) - \rho_m) A(z) \Delta z. \quad (6)$$

279 Eq. 6 incorporates gravity ($g = 9.81 \text{ m s}^{-2}$), depth (z), lake surface area (A_0), horizontal cross section area ($A(z)$),
280 lake density ($\rho(z)$), maximum depth (z_{\max}), mean lake density (ρ_m), lake volume (V) and volumetric mean depth
281 (z_m) defined as



$$z_m = \frac{1}{V} \sum_{z=0}^{z_{\max}} z A(z) \Delta z. \quad (7)$$

283 The duration of stratification was determined by counting the days when temperature differed by more than 1° C
284 between surface (2 m depth) and deep-water (280 m for LG; 50 m for LB) (Foley et al., 2012). The maximum
285 water column stability expression $N^2 = -(g/\rho) d\rho(z)/dz$ (s^{-2}) was used to determine the thermocline depth.

286 The river intrusion depth is dependent on water density (temperature and SSC). The Rhône is colder (Figs. 5c and
287 5d) and carries more suspended sediment (Figs. 5g and 5h) than Aare. Reference period results showed that the
288 Rhône intruded in LG at greater depths relative to depths of the Aare intrusion into LB (Figs. 8 and D1). Given
289 the future change in river temperature and SSC, intrusion patterns will thus change as the densities of both Aare
290 and Rhône increase and decrease during respective winter and summer seasons (section 3.1). This explains model
291 results showing respective deeper and shallower intrusions during winter and summer for both rivers (Fig. D1).

292 Model results show that warming of the Rhône generally diminishes the amount of river water penetrating beyond
293 200 m depth in LG (Fig. 8a). Elevated winter SSCs however increase river density. The combined effect of
294 temperature and SSC variation caused an increase in the amount of river water intruding beyond 200 m depth
295 (Fig. 8b). The difference in winter heating for the Aare and LB epilimnion (Figs. 5c, 5e and 6c) generally increased
296 the amount of water penetrating into the hypolimnion (Fig. 8c). Decommission of the MNPP enhances
297 temperature differentials between LB and the Aare, thereby increasing the amount of water reaching the deeper
298 parts of LB (Fig. 8d). In summary, the change in river discharge regime for the Aare and Rhône results in
299 respective increase and decrease in winter and summer water density, resulting in a summer to winter shift of the
300 amount of river water penetrating deeper than the metalimnion for both lakes.

301

302 **4 Discussion**

303 **4.1 Rivers**

304 Increases in air temperature expected from climate change modify tributary runoff. Less water is predicted to be
305 bound in snow and ice at high elevation during winter and spring/summer floods occur earlier (CH2011, 2011;
306 FOEN, 2012). The changed river discharge regime, appearing as increased flow in winter and decreased flow in
307 summer (Figs. 5a and 5b), amplifies the increase and decrease in river temperature during respective summer and
308 winter periods (Figs. 5e and 5f). Amplification results from (i) a smaller flow volume requiring less energy to heat
309 and (ii) lower flow velocities which extend heat exposure. The PREVAH model predict that the future discharge
310 of Aare in summer will be ~20% less than summer discharge predicted for the Rhône. Results therefore suggest
311 that the Aare summer conditions will be more impacted by climate change than Rhône summer conditions (Figs.
312 5e and 5f).

313 Model results concerning discharge-dependent responses to climate-induced warming were consistent with
314 previous findings reported by Isaak et al. (2012) and van Vliet et al. (2013). The river temperature increases
315 predicted by this study ($0.10^\circ \text{C decade}^{-1}$ for the Aare and $0.07^\circ \text{C decade}^{-1}$ for the Rhône) were much smaller than
316 past observed warming rates ($0.34^\circ \text{C decade}^{-1}$ for the Aare and $0.21^\circ \text{C decade}^{-1}$ for the Rhône; Hari et al., 2006).



317 These differences may reflect contrasting reference periods with past observations conducted from 1971 to 2001
318 and modelled observations addressing 1990 to 2099. Past observations also incorporate effects of solar brightening
319 during the 1980s (Fink et al., 2014a; Sanchez-Lorenzo and Wild, 2012; Wild et al., 2007).

320 Climate change effects aside, MNPP decommissioning in 2019 is predicted to decrease the temperature in the
321 Aare by up to 4.5°C at station #2085 (Råman Vinnå et al., 2017). The cooling effect of this plant closure primarily
322 affects winter conditions when climate change induced warming is weaker and river flow is lower (Fig. 5e). The
323 heating of Aare and LB by MNPP heat emissions equates to approximately one decade of climate-induced
324 warming of lake surface waters (O'Reilly et al., 2015; Råman Vinnå et al., 2017). This result highlights the role
325 of point source thermal contributions in local climate impact assessments. The effect is highly seasonally
326 dependent but persists into far-future time periods (Figs. 5c and 5e).

327 The amount of suspended sediment carried by rivers depends on both discharge and the amount of erodible
328 sediment in the watershed (Fink et al., 2016). We used a supply-based sediment rating model subjected to a
329 changing discharge regime to examine changes in suspended sediment from summer to winter for both Aare and
330 Rhône (Figs. 5g and 5h). Consistent with previous findings reported by Pralong et al. (2015), we predict an
331 increase in SSC during winter and decrease of SCC in summer.

332 Figure 4 and Table 2 show that the SSC model gives robust results for Rhône (coefficient of determination $R^2 =$
333 0.68 from 2013 to 2014) but not for Aare ($R^2 = 0.06$ from 2013 to 2014). The Aare includes several sediment-
334 trapping reservoirs/lakes upstream of station #2085. Peaks in SSC at station #2085 thus do not reflect watershed-
335 scale discharge events (Fig. 4) but rather local precipitation and discharge events in the headwaters of the Saane
336 River, a tributary to Aare (Fig. 2). This tributary hosts few sediment traps and contributes ~34% of the downstream
337 flow at station #2085. Given the limited impact of SSC on Aare water density, models show only negligible impact
338 on river intrusion depth and corresponding intruding volumes (Figs. 8c, B1c, B1e and D1c). The lower reaches of
339 the Rhône are not dammed, thus adhering more directly to model assumptions and giving clearer results (Fig. 4).

340 High SSC events are usually associated with extreme floods (Fink et al., 2016), which are predicted to vary in
341 alpine lake catchments with on-going climate change (Glur et al., 2013). The lack of constraints on extreme
342 precipitation events introduces uncertainty into future flood frequency and magnitude predictions (CH2011,
343 2011). Shifts in river discharge regimes also depend on the amount of water bound in snow and ice as well as on
344 the timing of spring/summer melt. Future climate scenarios predict that ~30% of the glacier mass will remain in
345 the Aare and Rhône catchments by the end of the 21st century (FOEN, 2012). Glacial meltwater is thus expected
346 to continue to supply the Aare and Rhône throughout the time frames considered in this study. We thus assumed
347 natural flood frequencies for our reference period and then adjusted them for overall river discharge regime shifts
348 predicted by FOEN (2012).

349

350 **4.2 Lakes**

351 All model scenarios showed that increased air temperature leads to warming of both lakes, especially of the
352 epilimnion (Table 5, Fig. 6). Piccolroaz et al. (2015) showed that an increase of lake stability and earlier onset of
353 stratification causes warming of surface waters due to the smaller volume undergoing warming and diminished



354 heat transfer to the hypolimnion. The lake model used here showed an increase of stratification strength and a
355 lengthening of the stratified period in both lakes (Table 5, Figs. 7g and 7h). Our results thus support consistently
356 previous findings for LG reported by Foley et al. (2012), O'Reilly et al. (2015) and Schwefel et al. (2016).

357 Seasonal variation in warming of both epilimnion and hypolimnion (Figs. 7a to 7f) exceeded that expected from
358 future changes in air temperature (Fig. 2a). The model showed a decrease in warming during winter and mid-
359 summer, which corresponds in time to periods of high river discharge from the main tributaries (Figs. 5a and 5b).
360 This cooling effect was more effective for LB than for LG (Fig. 7) and appeared in all scenarios except for LB1
361 and LG1 (Fig. C1), both of which exclude coupled river effects. The extended seasonal variation in climate
362 warming is thus driven by river discharge volume and temperature trends (Figs. 5 and 7). This response applies
363 to aquatic systems in which a difference exist in temperature and heating regimes between rivers and lakes, but
364 does not appear to affect water bodies with uniform temperature/heating regimes. Our results thus supports the
365 hypothesis put forward by Zhang et al. (2014), stating that climate warming of lakes might be reduced and even
366 reversed by addition of external water.

367 To investigate this effect, we varied the hydraulic residence time of LB and LG, while holding all other factors
368 constant (Fig. 9). We implemented a stepwise reduction in LG size (to 1/80 of its original volume), simultaneously
369 reducing hypsographic area but keeping maximum depth unchanged. Similar adjustments was made to LB to
370 obtain corresponding hydraulic residence times. This stepwise approach required 972 additional model runs.
371 These iterations showed that river water had to be cooler than lake water in order to generate the climate warming
372 dampening effect (Figs. 9a and 9d). Penetration into deep lake reaches by large river volumes strengthens the
373 effect in the hypolimnion (Fig. 9b). The climate dampening effect is suppressed when river and epilimnion
374 temperature are similar. MNPP thermal input creates such conditions in the Aare and therefore largely counteract
375 the river cooling effect of Aare on LB (Fig. 9c). For shorter residence times ($< \sim 1000$ days), rivers can exert
376 influence if a significant temperature difference exists between river and lake waters. For longer residence times
377 ($> \sim 1000$ days), tributaries cannot significantly offset climate effects in downstream water bodies.

378 Climate-induced warming of lakes (Schwefel et al., 2016), along with changing frequency or intensity of deep
379 penetrating flood events (Fink et al., 2016) may curtail oxygen supply to deep lakes. Recent flood analysis has
380 also indicated that input of river-borne organic matter increases respiration, causing a paradoxical net oxygen
381 deficit within the intruding layer (Bouffard and Perga, 2016). These findings highlight the necessity of estimating
382 the amount of oxygen saturated river water entering the hypolimnion. We therefore evaluated models
383 implementing climate-caused shifts in river discharge regimes for reaction of lakes and rivers to climate-induced
384 warming, shifts in seasonal SSC in rivers and local thermal pollution effects. Models showed respective winter
385 increase and summer decrease in river water density relative to lake stability. This creates summer to winter
386 seasonal shifts in deep intrusion dynamics for both lakes (Fig. D1). Models showed a net annual effect of increased
387 volumes of river water penetrating into deeper parts of both lakes (Fig. 8). An increase in winter SCC represented
388 the primary driver for increases in the amount of water annually penetrating past 200 m depth in LG (Figs. 8a, 8b
389 and D1a, D1b). In LB, colder winter river temperatures (relative to lake temperatures) due to removal of MNPP
390 heat contributed to greater penetration (Figs. 8c, 8d and D1c, D1d).



391 Fink et al. (2016) also found evidence that climate change will cause diminished deep river intrusion events in
392 summer and enhanced intrusion in winter. They predicted an annual decrease in the amount of river water reaching
393 the deepest parts of Lake Constance. The tributaries considered here differ from the Rhine River investigated by
394 Fink et al. (2016) primarily in terms of their temperature. The Rhône catchment for example rests at a mean
395 elevation of 2127 m and includes greater glacial coverage (11%) whereas the Rhine catchment rests at mean
396 elevation 1771 m and only has 1% glacial coverage. The closure of the MNPP and associated temperature decrease
397 contribute to increase of the volume/frequency of deep intrusion (Fig. 5). While Fink et al. (2016) focused
398 primarily on flood frequencies, our models emphasized river discharge regimes and interacting river and lake
399 temperature regimes. The annual increase in river penetration to depth predicted by our models suggests future
400 increase of deep-water oxygen supply in similar tributary-lake systems. This prediction applies primarily to
401 meromictic lakes such as LG. Analogous effects in holomictic lakes such as LB, which mix completely each
402 winter, are less significant. Similar to findings of Fink et al. (2016), our models indicate that deep-water oxygen
403 conditions will worsen during strongly stratified conditions due to seasonal shifts in deep river intrusions from
404 summer to winter.

405

406 **4.3 Model reliability**

407 Predictions concerning the effect of climate change on rivers and lakes depend on i) the choice of emission
408 scenario, ii) the accuracies of models linking climate to hydrology and climate to heat fluxes and iii) natural
409 variability of the system being investigated (Raymond Pralong et al., 2015). This section describes uncertainties
410 and limitations of our approach.

411 Results of long-term forecasts (beyond 2050) depend strongly on representations of global greenhouse gas (GHG)
412 emission scenarios (FOEN, 2012). Given uncertainties in future global climate policy, we chose a median
413 scenario, which falls between best (ex. RCP3PD) and the worst case scenarios (e.g. A2) in terms of GHG
414 emissions. A1B assumes a peak population at mid-century, balanced use of renewables and fossil fuels and rapid
415 introduction of new technologies.

416 Estimates of future air temperatures and river discharge were obtained from a combination of regional climate
417 models (RCMs; CH2011, 2011; FOEN, 2012). Uncertainties associated with individual RCMs were offset by
418 combined forecasts from multiple-model chains. Numerous studies have performed detailed evaluations of
419 uncertainty in air temperature and river discharge under established emission scenarios (RCP3PD, A1B, A2) and
420 accounting for global-regional climate model interactions (Addor et al., 2014; Bosshard et al., 2011, 2013;
421 CH2011, 2011).

422 The degree of accuracy with which model input parameters represent future conditions determines the accuracy
423 of model predictions. We therefore ran the river temperature model with varying parameters to evaluate model
424 sensitivity (Table 1) for different yet similar datasets. The air2stream parameter a_1 showed the greatest degree of
425 sensitivity, varying within three orders of magnitude. The a_1 parameter, however, does not respond to variation in
426 river discharge or air temperature (Equation 1), which limits its sensitivity to climatic input data. The other
427 parameters (a_2 to a_8) varied only within one order of magnitude (Table 1). The SSC model gives better results for
428 the Rhône (coefficient of determination $R^2 = 0.68$ from 2013 to 2014) than for the Aare ($R^2 = 0.06$ from 2013 to



429 2014). Dam and reservoir infrastructure upstream of station #2085 along the Aare dampen sediment transport
430 events and decouple them from regional discharge events (see above; Fig. 4). Given the relatively minor effect of
431 SSC on Aare water density, variation in the input parameter does not influence river intrusion depth estimates
432 (Figs. B1e to B1f and D1c to D1d). Previous studies have evaluated the accuracy of SIMSTRAT lake model
433 predictions based on climatic data (Schwefel et al., 2016) and anthropogenic thermal emissions (Fink et al., 2014b;
434 Råman Vinnå et al., 2017). As with other vertical, one-dimensional models, SIMSTRAT cannot account for lateral
435 heterogeneities in lakes. This inherent weakness in model design however does not significantly diminish the
436 accuracy of model predictions concerning LB and LG (Råman Vinnå et al., 2017; Schwefel et al., 2016).

437 This study assumes that glacial melt-water feeding both the Aare and Rhône in summer will not disappear within
438 the time frames considered here. Loss of glacial sources would drastically modify the assumed discharge regime,
439 especially in summer, which would affect accuracy of temperature, SSC and intrusion depth estimates presented
440 here. However, as stated in section 4.1, FOEN (2012) predicts that the Aare and Rhône catchments will retain
441 30% of their glacial masses by the year 2100. These predictions support assumptions concerning the Aare and
442 Rhône discharge regimes used here. Point sources/sinks of anthropogenic heat can affect inland water bodies
443 response to climate change, as shown by the MNPP effects described here. Other changes in catchment
444 management, such as hydropower dam construction would also likely alter river discharge regimes and by
445 extension, temperatures, SSCs and deep-water renewal (Fink et al., 2016). The accuracy of future climate change
446 predictions depends on accurate accounting of regional anthropogenic factors affecting physical processes in the
447 system under investigation.

448

449 **5 Conclusion**

450 Aquatic processes in lakes are the result of regional climate and events in upstream tributaries. This study
451 investigated the impact of climate change on inland waters by propagating climatic inputs through integrated
452 fluvial-lacustrine systems. We entered predicted future climatic data into models for two connected river and lake
453 systems in order to evaluate downstream thermal responses and how river discharge regime shifts might affect
454 deep-water renewal in the lakes. Climate data propagated through discharge-dependent river temperature and
455 suspended sediment concentration models coupled to a one-dimensional lake model yielded theoretical hydrologic
456 predictions for two peri-alpine lakes, Lake Biel and Lake Geneva.

457 The models showed that climate warming of rivers is enhanced in summer and diminished in winter due to future
458 river discharge regimes with decreased flow in summer and increased flow in winter. This climate-caused
459 alteration of the flow regime likewise increases the river-borne suspended sediment load in winter and decreases
460 it in summer.

461 Both lakes showed large seasonal temperature increases that could not be solely explained by climate-related
462 (predicted) increases in air temperature. Instead, the lakes experienced a cooling effect associated with upstream
463 tributaries, whose response to increasing future air temperatures differed from that of the lakes. The smaller Lake
464 Biel showed increased response to this repressive effect on climate warming than that of the larger Lake Geneva.
465 Predicted changes in Lake Biel strongly depend on removal of upstream anthropogenic thermal emission into the
466 Aare River. Local anthropogenic point sources of heat can thus rival climate change in terms of their influence on



467 lakes. This dampening of climate warming depends on the lakes hydraulic residence times and requires adequate
468 river/lake temperature differences. Our models indicate that tributaries can exert system-wide influence on lakes
469 with hydraulic residence times $< \sim 1000$ days. Lake systems with longer residence times are resistant to tributary
470 effects but may respond to local effects.

471 The combination of changes in river SSC and differential lake/river temperature/warming result in a seasonal shift
472 of deep-water penetration (by rivers) into lakes. The volume of river water penetrating to deeper parts of lakes
473 specifically decreases in summer and increases in winter. The net effect of these predicted shifts enhances annual
474 deep-water renewal. Higher rates of deep-water renewal can in turn enhance reoxygenation of the deepest reaches
475 of lakes, which may otherwise experience lower oxygen concentrations under climate change.

476

477 Data availability

478 See acknowledgments

479

480 Appendices

481 Appendix A1 River Intrusion Model

482 Figure A1 summarizes the river intrusion model. The depth where the river plume separates from the surface, the
483 so-called plunge depth (h_p), depends on the slope angle (σ), gravity (g), coefficients ($S_1 = 0.25$; $S_2 = 0.75$; Ellison
484 and Turner, 1959), bed friction ($f_t = 0.02$; Akiyama and Heinz, 1984), initial flow per unit width ($q_0 = V_r / W_r$
485 dependent on river discharge (V_r), river width ($W_r = 100$ m for the Aare and $W_r = 120$ m for the Rhône) and the
486 relative density difference ($\Delta\rho = (\rho_r - \rho_l(z_1)) / \rho_l(z_1)$) between the homogenous river (ρ_r) and lake (ρ_l) with $z_1 =$
487 surface.

$$488 \quad h_p = e_1 \left(\frac{f_t}{\sigma(z) S_2} \frac{q_0^2}{g \Delta\rho} \right)^{1/3} + e_2 \left(\frac{q_0^2}{S_1 g \Delta\rho} \right)^{1/3} \quad (\text{A1})$$

489 The level of initial plume entrainment is treated differently on a gentle versus a steep slope. This is controlled by
490 the coefficients e_1 and e_2 .

$$491 \quad e_1 = \begin{cases} 1: \sigma(z_1) < \sigma_c \\ 0: \sigma(z_1) \geq \sigma_c \end{cases} \quad (\text{A2})$$

$$492 \quad e_2 = \begin{cases} 0: \sigma(z_1) < \sigma_c \\ 1: \sigma(z_1) \geq \sigma_c \end{cases} \quad (\text{A3})$$

493 where the critical slope angle ($\sigma_c = f_t S_1 / S_2$) distinguishes between gentle and steep slope designations. The initial
494 height of the underflow (h_d) can then be written as



$$495 \quad h_d(z_1) = h_p(1 + \gamma) \quad (A4)$$

496 where γ is the entrance mixing coefficient equal to ~ 0 for gentle slopes and increasing to larger values for steeper
497 slopes. Here we find that a value of 0.1 provides best result. The initial underflow temperature (T_u), velocity (U_u),
498 particle content (P_u) and volume (V_u) is consequently expressed as a function of ambient lake water temperature
499 (T_i), river temperature (T_r) and river particle content (P_r) in the homogenous region.

$$500 \quad T_u(z_1) = T_i(z_1) \frac{(h_d(z_1) - h_p)}{h_d(z_1)} + T_r \frac{h_p}{h_d(z_1)} \quad (A5)$$

$$501 \quad U_u(z_1) = (1 + \gamma) \frac{q_0}{h_d(z_1)} \quad (A6)$$

$$502 \quad P_u(z_1) = P_r \frac{h_p}{h_d(z_1)} \quad (A7)$$

$$503 \quad V_u(z_1) = V_r \frac{h_p}{h_d(z_1)} \quad (A8)$$

504 Once the plume has passed through the plunge region into the underflow region, we express h_d , U_u , T_u and V_u as

$$505 \quad h_d(z+1) = h_d(z) + E(z)dx \quad (A9)$$

$$506 \quad U_u(z+1) = U_u(z) \frac{h_d(z)}{h_d(z+1)} \quad (A10)$$

$$507 \quad T_u(z+1) = T_i(z) \frac{(h_d(z+1) - h_d(z))}{h_d(z+1)} + T_u(z) \frac{h_d(z)}{h_d(z+1)} \quad (A11)$$

$$508 \quad V_u(z+1) = V_u(z) \frac{h_d(z)}{h_d(z+1)} \quad (A12)$$

509 where dx is the horizontal distance between z and $z+1$ and the entrainment factor (E) is expressed as a function
510 of the entrainment constant ($\beta = 0.0015$; Ashida and Egashira, 1975) and the Richardson number (R_i).

511

$$512 \quad E(z) = \frac{\beta}{R_i(z)} \quad (A13)$$

$$513 \quad R_i(z) = \frac{f_t}{\sigma(z)S_2} \quad (A14)$$



514 For P_u , we include a sedimentation term as proposed by Syvitski and Lewis (1992), which depends on the removal
515 rate (r) and $dt = dx / U_u(z)$.

$$516 \quad P_u(z+1) = P_u(z) \frac{h_d(z)}{h_d(z+1)} - re_3 h_d(z) P_u(z) e^{-rdt} \quad (A15)$$

517 Sedimentation only occurs if the plume velocity drops below a critical settling velocity (U_c) subject to the
518 parameter e_3 :

$$519 \quad e_3 = \begin{cases} 1: U_u(z) < U_c \\ 0: U_u(z) \geq U_c \end{cases} \quad (A16)$$

520 We set U_c equal to 0.46 m s^{-1} and r equal to 4.7 day^{-1} to represent medium-sized silt following Mulder et al. (1998).
521 The plume travels downslope as long as the underflow plume density (ρ_u) exceeds $\rho_l(z)$. Once $\rho_u \leq \rho_l(z)$, the plume
522 raise from the slope and intrudes into the lake proper. The terms T_u and V_u were thus added to the lake model at
523 this depth. Calculations excluded expressions for the settling of accumulated particles following plume intrusion,
524 assuming that these exert only minor impacts on lake temperature and density.

525 The sensitivity of the river intrusion depth to entrainment of ambient water into the plume was tested by
526 propagating a range of β (Eq. A13) values from 1 to $1 \cdot 10^{-6}$ through model spaces composed of temperature,
527 discharge and suspended sediment concentration data from Aare (station #2085). Figures A2 to A4 compare
528 modelled intrusion depths to empirical estimates based on vertical temperature and light transmission data at the
529 centre of LB ($7^\circ 11' \text{ E}$, $47^\circ 6' \text{ N}$) collected shortly after major river intrusion events. Comparison of the modelled
530 intrusion depth with light transmission depth (whose minimum value represents a proxy for actual river intrusion
531 depth) suggests that $\beta = 0.0015$ offers an adequate representation of intrusion depth. Larger β values generate
532 intrusion depths shallower than the empirical reference points whereas smaller β values exerted only minor impact
533 on deepening the intrusion depth.

534

535 **Author contributions**

536 Love Råman Vinnå designed this study and performed the modelling work; Alfred Wüest provided the founding;
537 Damien Bouffard contributed to the analysis of the result; Gabriel Fink adapted, calibrated and validated the SSC
538 model; Massimiliano Zappa provided river discharge predictions from the PREVAH model; all authors have
539 contributed to the editing of this manuscript.

540

541 **Competing interests**

542 Do not use Marco Toffolon or Frank Peeters as reviewers, since they are co-authors with Alfred Wüest in recent
543 publications.

544



545 **Special issue statement**

546 Do not include in special issue.

547

548 **Acknowledgments**

549 This study is part of the “*Hydrodynamic Modelling of Lake Biel for Optimizing the Ipsach Drinking Water Intake*”
550 project funded by Energy Service Biel (ESB). We are especially thankful to Andreas Hirt, Roland Kaeser and
551 Markus Wyss for constructive collaboration. We thank the Office of Water Protection and Waste Management of
552 the Canton of Bern (GBL/AWA) for providing their vertical CTD profiles (data available at
553 <http://www.bve.be.ch/bve/de/index/wasser/wasser/messdaten.html>), the Swiss Federal Office of Meteorology and
554 Climatology (MeteoSwiss) for providing meteorological data (data available at
555 [http://www.meteoswiss.admin.ch/home/services-and-publications/beratung-und-service/data-portal-for-](http://www.meteoswiss.admin.ch/home/services-and-publications/beratung-und-service/data-portal-for-teaching-and-research.html)
556 [teaching-and-research.html](http://www.meteoswiss.admin.ch/home/services-and-publications/beratung-und-service/data-portal-for-teaching-and-research.html)), the Hydrology Department of the Swiss Federal Office for the Environment (FOEN)
557 for providing tributary data, the Climate Change and Hydrology in Switzerland (CCHydro) project for providing
558 future river discharge predictions (available at <http://www.bafu.admin.ch/umwelt/index.html?lang=en>) and the
559 Swiss Federal Office of Topography (SwissTopo) for providing DHM25 model bathymetry data (available at
560 https://shop.swisstopo.admin.ch/en/products/height_models/dhm25). We thank Bettina Schaepli at the University
561 of Lausanne, Marco Toffolon and Elisa Calamita at the University of Trento, Robert Schwefel at École
562 Polytechnique Fédérale de Lausanne, Adrien Gaudard at the Swiss Federal Institute of Aquatic Science and
563 Technology and Stan Thorez at the University of Eindhoven for valuable insights and help with model setup. We
564 furthermore thank Kei Ito (http://jfly.iam.u-tokyo.ac.jp/html/color_blind/) for valuable feedback on how to adapt
565 our figures for colour-blind readership.

566

567 **References**

- 568 Addor, N., Rössler, O., Köplin, N., Huss, M., Weingartner, R. and Seibert, J.: Robust changes and sources of
569 uncertainty in the projected hydrological regimes of Swiss catchments, *Water Resour. Res.*, 50(10), 7541–7562,
570 doi:10.1002/2014WR015549, 2014.
- 571 Akiyama, J. and Heinz, S. G.: Plunging flow into a reservoir: theory, *J. Hydraul. Eng.*, 10(110), 484–499, 1984.
- 572 Ashida, K. and Egashira, S.: Basic study on turbidity currents, *Proc. Jpn. Soc. Civ. Eng.*, 1975(237), 37–50, 1975.
- 573 Austin, J. A. and Colman, S. M.: Lake Superior summer water temperatures are increasing more rapidly than
574 regional air temperatures: A positive ice-albedo feedback, *Geophys. Res. Lett.*, 34(6), L06604,
575 doi:10.1029/2006GL029021, 2007.
- 576 Bennett, G. L., Molnar, P., McArdeell, B. W., Schlunegger, F. and Burlando, P.: Patterns and controls of sediment
577 production, transfer and yield in the Illgraben, *Geomorphology*, 188, 68–82,
578 doi:10.1016/j.geomorph.2012.11.029, 2013.
- 579 Birsan, M.-V., Molnar, P., Burlando, P. and Pfaundler, M.: Streamflow trends in Switzerland, *J. Hydrol.*, 314(1–
580 4), 312–329, doi:10.1016/j.jhydrol.2005.06.008, 2005.
- 581 Bosshard, T., Kotlarski, S., Ewen, T. and Schär, C.: Spectral representation of the annual cycle in the climate
582 change signal, *Hydrol. Earth Syst. Sci.*, 15(9), 2777–2788, doi:10.5194/hess-15-2777-2011, 2011.
- 583 Bosshard, T., Carambia, M., Goergen, K., Kotlarski, S., Krahe, P., Zappa, M. and Schär, C.: Quantifying
584 uncertainty sources in an ensemble of hydrological climate-impact projections, *Water Resour. Res.*, 49(3), 1523–
585 1536, doi:10.1029/2011WR011533, 2013.
- 586 Bouffard, D. and Perga, M.-E.: Are flood-driven turbidity currents hot-spots for priming effect in lakes?
587 *Biogeosciences*, 13, 3573–3584, doi:10.5194/bg-13-3573-2016, 2016.
- 588 Caissie, D.: The thermal regime of rivers: a review, *Freshw. Biol.*, 51(8), 1389–1406, doi:10.1111/j.1365-
589 2427.2006.01597.x, 2006.
- 590 CH2011: Swiss climate change scenarios CH2011, published by C2SM, MeteoSwiss, ETH, NCCR Climate, and
591 OcCC, Zurich, Switzerland, 88 pp. ISBN: 978-3-033-03065-7., 2011.
- 592 Doomen, A. M. C., Wijma, E., Zwolsman, J. J. G. and Middelkoop, H.: Predicting suspended sediment
593 concentrations in the Meuse river using a supply-based rating curve, *Hydrol. Process.*, 22(12), 1846–1856,
594 doi:10.1002/hyp.6767, 2008.
- 595 Downing, J. A., Prairie, Y. T., Cole, J. J., Duarte, C. M., Tranvik, L. J., Striegl, R. G., McDowell, W. H.,
596 Kortelainen, P., Caraco, N. F., Melack, J. M. and others: The global abundance and size distribution of lakes,
597 ponds, and impoundments, *Limnol. Oceanogr.*, 51(5), 2388–2397, 2006.
- 598 Ellison, T. H. and Turner, J. S.: Turbulent entrainment in stratified flows, *J. Fluid Mech.*, 6(03), 423–448,
599 doi:10.1017/S0022112059000738, 1959.
- 600 Federal Office for the Environment FOEN (publ.): Effects of climate change on water resources and waters,
601 Synthesis report on “Climate Change and Hydrology in Switzerland” (CCHydro) project, Federal Office for the
602 Environment, Bern. Umwelt-Wissen No 1217: 74 S., 2012.
- 603 Fenocchi, A., Rogora, M., Sibilla, S. and Dresti, C.: Relevance of inflows on the thermodynamic structure and on
604 the modeling of a deep subalpine lake (Lake Maggiore, Northern Italy/Southern Switzerland), *Limnol. - Ecol.
605 Manag. Inland Waters*, 63, 42–56, doi:10.1016/j.limno.2017.01.006, 2017.
- 606 Fink, G., Schmid, M., Wahl, B., Wolf, T. and Wüest, A.: Heat flux modifications related to climate-induced
607 warming of large European lakes, *Water Resour. Res.*, 50(3), 2072–2085, doi:10.1002/2013WR014448, 2014a.



- 608 Fink, G., Schmid, M. and Wüest, A.: Large lakes as sources and sinks of anthropogenic heat: Capacities and
609 limits, *Water Resour. Res.*, 50(9), 7285–7301, doi:10.1002/2014WR015509, 2014b.
- 610 Fink, G., Wessels, M. and Wüest, A.: Flood frequency matters: Why climate change degrades deep-water quality
611 of peri-alpine lakes, *J. Hydrol.*, 540, 457–468, doi:10.1016/j.jhydrol.2016.06.023, 2016.
- 612 Foley, B., Jones, I. D., Maberly, S. C. and Rippey, B.: Long-term changes in oxygen depletion in a small temperate
613 lake: Effects of climate change and eutrophication: Oxygen depletion in a small lake, *Freshw. Biol.*, 57(2), 278–
614 289, doi:10.1111/j.1365-2427.2011.02662.x, 2012.
- 615 Gaudard, A., Schwefel, R., Råman Vinnå, L., Schmid, M., Wüest, A. and Bouffard, D.: Optimizing the
616 parameterization of deep mixing and internal seiches in one-dimensional hydrodynamic models: a case study with
617 Simstrat, *Geosci. Model Dev. Discuss.*, 1–18, doi:10.5194/gmd-2016-262, 2016.
- 618 Gillet, C. and QueTin, P.: Effect of temperature changes on the reproductive cycle of roach in Lake Geneva from
619 1983 to 2001, *J. Fish Biol.*, 69(2), 518–534, doi:10.1111/j.1095-8649.2006.01123.x, 2006.
- 620 Glur, L., Wirth, S. B., Büntgen, U., Gilli, A., Haug, G. H., Schär, C., Beer, J. and Anselmetti, F. S.: Frequent
621 floods in the European Alps coincide with cooler periods of the past 2500 years, *Sci. Rep.*, 3, 2770,
622 doi:10.1038/srep02770, 2013.
- 623 Goudsmit, G.-H., Burchard, H., Peeters, F. and Wüest, A.: Application of k-ε turbulence models to enclosed
624 basins: The role of internal seiches, *J. Geophys. Res.*, 107(C12), 3230, doi:10.1029/2001JC000954, 2002.
- 625 Hari, R. E., Livingstone, D. M., Siber, R., Burkhardt-Holm, P. and Guettinger, H.: Consequences of climatic
626 change for water temperature and brown trout populations in Alpine rivers and streams, *Glob. Change Biol.*, 12,
627 10–26, doi:10.1111/j.1365-2486.2005.01051.x, 2006.
- 628 Holgerson, M. A. and Raymond, P. A.: Large contribution to inland water CO₂ and CH₄ emissions from very
629 small ponds, *Nat. Geosci.*, 9(3), 222–226, doi:10.1038/ngeo2654, 2016.
- 630 Isaak, D. J., Wollrab, S., Horan, D. and Chandler, G.: Climate change effects on stream and river temperatures
631 across the northwest U.S. from 1980–2009 and implications for salmonid fishes, *Clim. Change*, 113(2), 499–524,
632 doi:10.1007/s10584-011-0326-z, 2012.
- 633 Kirillin, G.: Modeling the impact of global warming on water temperature and seasonal mixing regimes in small
634 temperate lakes, *Boreal Env. Res.*, 15, 279–293, 2010.
- 635 Kirillin, G., Shatwell, T. and Kasprzak, P.: Consequences of thermal pollution from a nuclear plant on lake
636 temperature and mixing regime, *J. Hydrol.*, 496, 47–56, doi:10.1016/j.jhydrol.2013.05.023, 2013.
- 637 Kobiarska, F., Jonas, T., Magnusson, J., Zappa, M., Bavay, M., Bosshard, T., Paul, F. and Bernasconi, S. M.:
638 Climate change effects on snow melt and discharge of a partly glacierized watershed in Central Switzerland
639 (SoilTrec Critical Zone Observatory), *Appl. Geochem.*, 26, S60–S62, doi:10.1016/j.apgeochem.2011.03.029,
640 2011.
- 641 Mulder, T., Syvitski, J. P. M. and Skene, K. I.: Modeling of erosion and deposition by turbidity currents generated
642 at river mouths, *J. Sediment. Res.*, 68(1), 124–137, doi:10.2110/jsr.68.124, 1998.
- 643 O'Reilly, C. M., Sharma, S., Gray, D. K., Hampton, S. E., Read, J. S., Rowley, R. J., Schneider, P., Lenters, J. D.,
644 McIntyre, P. B., Kraemer, B. M., Weyhenmeyer, G. A., Straile, D., Dong, B., Adrian, R., Allan, M. G., Anneville,
645 O., Arvola, L., Austin, J., Bailey, J. L., Baron, J. S., Brookes, J. D., de Eyto, E., Dokulil, M. T., Hamilton, D. P.,
646 Havens, K., Hetherington, A. L., Higgins, S. N., Hook, S., Izmet'eva, L. R., Joehnk, K. D., Kangur, K., Kasprzak,
647 P., Kumagai, M., Kuusisto, E., Leshkevich, G., Livingstone, D. M., MacIntyre, S., May, L., Melack, J. M.,
648 Mueller-Navarra, D. C., Naumenko, M., Noges, P., Noges, T., North, R. P., Plisnier, P.-D., Rigosi, A., Rimmer,
649 A., Rogora, M., Rudstam, L. G., Rusak, J. A., Salmaso, N., Samal, N. R., Schindler, D. E., Schladow, S. G.,
650 Schmid, M., Schmidt, S. R., Silow, E., Soylu, M. E., Teubner, K., Verburg, P., Voutilainen, A., Watkinson, A.,
651 Williamson, C. E. and Zhang, G.: Rapid and highly variable warming of lake surface waters around the globe,
652 *Geophys Res Lett*, 42(24), 10,773–10,781, doi:10.1002/2015GL066235, 2015.



- 653 Pachauri, R. K., Mayer, L. and Intergovernmental Panel on Climate Change, Eds.: Climate change 2014: synthesis
654 report, Intergovernmental Panel on Climate Change, Geneva, Switzerland., 2015.
- 655 Peeters, F., Livingstone, D. M., Goudsmit, G.-H., Kipfer, R. and Forster, R.: Modeling 50 years of historical
656 temperature profiles in a large central European lake, *Limnol. Oceanogr.*, 47(1), 186–197,
657 doi:10.4319/lo.2002.47.1.0186, 2002.
- 658 Perroud, M. and Goyette, S.: Impact of warmer climate on Lake Geneva water-temperature profiles, *Boreal*
659 *Environ. Res.*, 15, 255–278, 2010.
- 660 Piccolroaz, S., Toffolon, M. and Majone, B.: The role of stratification on lakes' thermal response: The case of
661 Lake Superior, *Water Resour. Res.*, 51, 7878–7894, doi:10.1002/2014WR016555, 2015.
- 662 Råman Vinnå, L., Wüest, A. and Bouffard, D.: Physical effects of thermal pollution in lakes, *Water Resour. Res.*,
663 53, doi:10.1002/2016WR019686, 2017.
- 664 Raymond Pralong, M., Turowski, J. M., Rickenmann, D. and Zappa, M.: Climate change impacts on bedload
665 transport in alpine drainage basins with hydropower exploitation: climate change impacts on bedload transport,
666 *Earth Surf. Process. Landf.*, 40(12), 1587–1599, doi:10.1002/esp.3737, 2015.
- 667 Rimmer, A. and Hartmann, A.: Optimal hydrograph separation filter to evaluate transport routines of hydrological
668 models, *J. Hydrol.*, 514, 249–257, doi:10.1016/j.jhydrol.2014.04.033, 2014.
- 669 Sanchez-Lorenzo, A. and Wild, M.: Decadal variations in estimated surface solar radiation over Switzerland since
670 the late 19th century, *Atmospheric Chem. Phys.*, 12(18), 8635–8644, doi:10.5194/acp-12-8635-2012, 2012.
- 671 Schmidt, W.: Über die Temperatur- und Stabilitätsverhältnisse von Seen, *Geogr. Ann.*, 10, 145–177,
672 doi:10.2307/519789, 1928.
- 673 Schwefel, R., Gaudard, A., Wüest, A. and Bouffard, D.: Effects of climate change on deepwater oxygen and
674 winter mixing in a deep lake (Lake Geneva): Comparing observational findings and modeling, *Water Resour.*
675 *Res.*, 52(11), 8811–8826, doi:10.1002/2016WR019194, 2016.
- 676 Speich, M. J. R., Bernhard, L., Teuling, A. J. and Zappa, M.: Application of bivariate mapping for hydrological
677 classification and analysis of temporal change and scale effects in Switzerland, *J. Hydrol.*, 523, 804–821,
678 doi:10.1016/j.jhydrol.2015.01.086, 2015.
- 679 Syvitski, J. P. M. and Lewis, A. G.: The seasonal distribution of suspended particles and their iron and manganese
680 loading in a glacial runoff fiord, *Geosci. Can.*, 19(1), 13–20, 1992.
- 681 Tananaev, N. I.: Hysteresis effect in the seasonal variations in the relationship between water discharge and
682 suspended load in rivers of permafrost zone in Siberia and Far East, *Water Resour.*, 39(6), 648–656,
683 doi:10.1134/S0097807812060073, 2012.
- 684 Toffolon, M. and Piccolroaz, S.: A hybrid model for river water temperature as a function of air temperature and
685 discharge, *Environ. Res. Lett.*, 10(11), 114011, doi:10.1088/1748-9326/10/11/114011, 2015.
- 686 Toffolon, M., Piccolroaz, S., Majone, B., Soja, A.-M., Peeters, F., Schmid, M. and Wüest, A.: Prediction of surface
687 temperature in lakes with different morphology using air temperature, *Limnol. Oceanogr.*, 59(6), 2185–2202,
688 doi:10.4319/lo.2014.59.6.2185, 2014.
- 689 Van Vliet, M. T. H., Franssen, W. H. P., Yearsley, J. R., Ludwig, F., Haddeland, I., Lettenmaier, D. P. and Kabat,
690 P.: Global river discharge and water temperature under climate change, *Glob. Environ. Change*, 23(2), 450–464,
691 doi:10.1016/j.gloenvcha.2012.11.002, 2013.
- 692 Viviroli, D., Zappa, M., Gurtz, J. and Weingartner, R.: An introduction to the hydrological modelling system
693 PREVAH and its pre- and post-processing-tools, *Environ. Model. Softw.*, 24(10), 1209–1222,
694 doi:10.1016/j.envsoft.2009.04.001, 2009.



- 695 Wahl, B. and Peeters, F.: Effect of climatic changes on stratification and deep-water renewal in Lake Constance
696 assessed by sensitivity studies with a 3D hydrodynamic model, *Limnol. Oceanogr.*, 59(3), 1035–1052,
697 doi:10.4319/lo.2014.59.3.1035, 2014.
- 698 Wild, M., Ohmura, A. and Makowski, K.: Impact of global dimming and brightening on global warming,
699 *Geophys. Res. Lett.*, 34, L04702, doi:10.1029/2006GL028031, 2007.
- 700 Williamson, C. E., Overholt, E. P., Pilla, R. M., Leach, T. H., Brentrup, J. A., Knoll, L. B., Mette, E. M. and
701 Moeller, R. E.: Ecological consequences of long-term browning in lakes, *Sci. Rep.*, 5, 18666,
702 doi:10.1038/srep18666, 2015.
- 703 Wright, S. A., Holly Jr, F. M., Bradley, A. A. and Krajewski, W.: Long-term simulation of thermal regime of
704 Missouri River, *J. Hydraul. Eng.*, 125(3), 242–252, 1999.
- 705 Zhang, G., Yao, T., Xie, H., Qin, J., Ye, Q., Dai, Y. and Guo, R.: Estimating surface temperature changes of lakes
706 in the Tibetan Plateau using MODIS LST data: WST over the TP, *J. Geophys. Res. Atmospheres*, 119(14), 8552–
707 8567, doi:10.1002/2014JD021615, 2014.
- 708 Zhong, Y., Notaro, M., Vavrus, S. J. and Foster, M. J.: Recent accelerated warming of the Laurentian Great Lakes:
709 Physical drivers, *Limnol. Oceanogr.*, 61(5), 1762–1786, doi:10.1002/lno.10331, 2016.
- 710

711 **Tables**

712 **Table 1.** Air2stream river temperature model best-fit parameters and model
713 performance statistics reported as coefficients of determination (R^2) and
714 root mean square deviation (RMSD). Input parameters used in this study
715 are shown in bold-faced type. The model was calibrated, validated and
716 subjected to sensitivity tests using data from station #2085 (Aare River)
717 representing past observed conditions and future predicted conditions
718 assuming MNPP removal (No MNPP).

Parameter (Unit)	Aare (#2085)		Rhône (#2009)
	Measurements	No MNPP	Measurements
a_1 ($^{\circ}\text{C s}^{-1}$)	2.0316	0.6434	1.4927
a_2 (s^{-1})	0.2299	0.3855	0.2774
a_3 (s^{-1})	0.2267	0.3177	0.4133
a_4 (-)	0.0157	0.5622	0.6399
a_5 ($^{\circ}\text{C s}^{-1}$)	6.7022	16.2387	6.4792
a_6 ($^{\circ}\text{C s}^{-1}$)	4.4950	9.9855	2.3224
a_7 (-)	0.6066	0.6066	0.5244
a_8 (s^{-1})	0.7156	1.5930	1.0760
		R^2 (-)	
Calibration ^a	0.97	0.96	0.94
Validation ^b	0.95	0.96	0.94
	RMSD ($^{\circ}\text{C}$)		
Calibration ^a	0.83	0.95	0.52
Validation ^b	1.02	1.06	0.59

719 ^a 1990 - 1999720 ^b 2000 - 2009

721



722 **Table 2.** River suspended sediment concentration
 723 (SSC) model best-fit parameters and model
 724 performance statistics reported as coefficients of
 725 determination (R^2) and root mean square deviation
 726 (RMSD).

Parameter (Unit)	Aare (#2085)	Rhône (#2009)
m (g m^{-3})	8.8000	1.0000
b_1 (g s m^{-6})	0.2650	0.0006
c_1 (-)	0.6500	2.3200
b_2 (g s m^{-6})	0.0011	0.0010
c_2 (-)	2.3000	12.0000
b_3 (g m^{-3})	8.8000	2.0000
Q_{th} ($\text{m}^3 \text{s}^{-1}$)	401	232
	R^2 (-)	
Calibration ^a	0.20	0.74
Validation ^b	0.03	0.58
	RMSD (g m^{-3})	
Calibration ^a	82	206
Validation ^b	217	222

727 ^a 2013

728 ^b 2014

729



730 **Table 3.** One-dimensional lake model
731 SIMSTRAT best-fit parameters and model
732 performance statistics reported as vertical
733 volume-weighted averaged root mean square
734 deviation (RMSD-V).

Parameter (Unit)	Lake Biel	Lake Geneva
p_1 (-)	1.30	1.09
p_2 (-)	1.20	0.90
K (-)	0.70	1.40
q (-)	1.30	1.25
C_{Defl} (-)	0.0050	0.0020
C_{10} (-)	0.0016	0.0017
a_s (-)	0.0060	0.035
a_w (-)	0.0040	0.009
RMSD-V (°C)		
Calibration	0.73 ^a	0.66 ^c
Validation	0.68 ^b	

735 ^a 1995 - 2004

736 ^b 2005 - 2015

737 ^c 1981 - 2012

738

739 **Table 4.** Model scenarios of climate change effects for near-future and far-future time
740 periods, including (Inc.) and excluding (Exc.) the effects of rivers and suspended
741 sediment. Thermal input from MNPP also included/excluded. Most likely scenarios
742 shown in bold.

Lake	Exc. Rivers	Inc. Rivers	
		Exc. Suspended Sediment	Inc. Suspended Sediment
Geneva	LG1	LG2	LG3
		Inc. MNPP	Exc. MNPP
Biel	LB1	LB2	LB3

743



744 **Table 5.** Change in temperature, length of the stratified period and depth of the thermocline
 745 (negative values correspond to a shallower thermocline) for each scenario listed in Table 4.
 746 Estimates given as mean of the daily difference between the reference period and the far-future time
 747 period. Temperature anomalies are volume-weighted and vertically averaged. Most likely scenarios
 748 shown in bold.

Scenario	Temperature (°C decade ⁻¹)			Stratification (days decade ⁻¹)	Thermocline (m decade ⁻¹)
	Epilimnion	Metalimnion	Hypolimnion		
Lake Biel					
LB1	0.19	0.16	0.13	1.5	-0.02
LB2	0.15	0.13	0.06	2.0	-0.07
LB3	0.13	0.11	0.05	2.2	-0.13
Lake Geneva					
LG1	0.17	0.13	0.07	2.9	-0.07
LG2	0.17	0.12	0.07	2.8	-0.06
LG3	0.18	0.16	0.08	2.2	-0.04

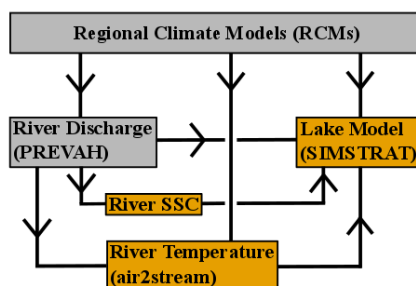
749

750

751



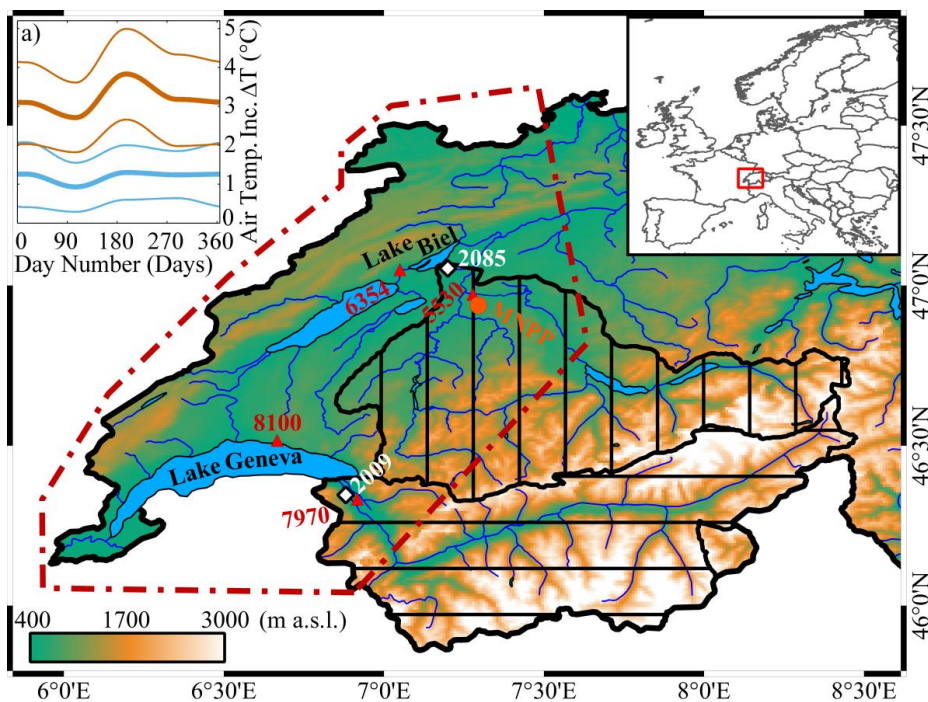
752 **Figures**



753

754 **Figure 1.** Schematic illustration of this study's one-way model chain. Orange models represent modeling
 755 performed by this study while grey models represent simulated data inputs obtained from external sources.

756



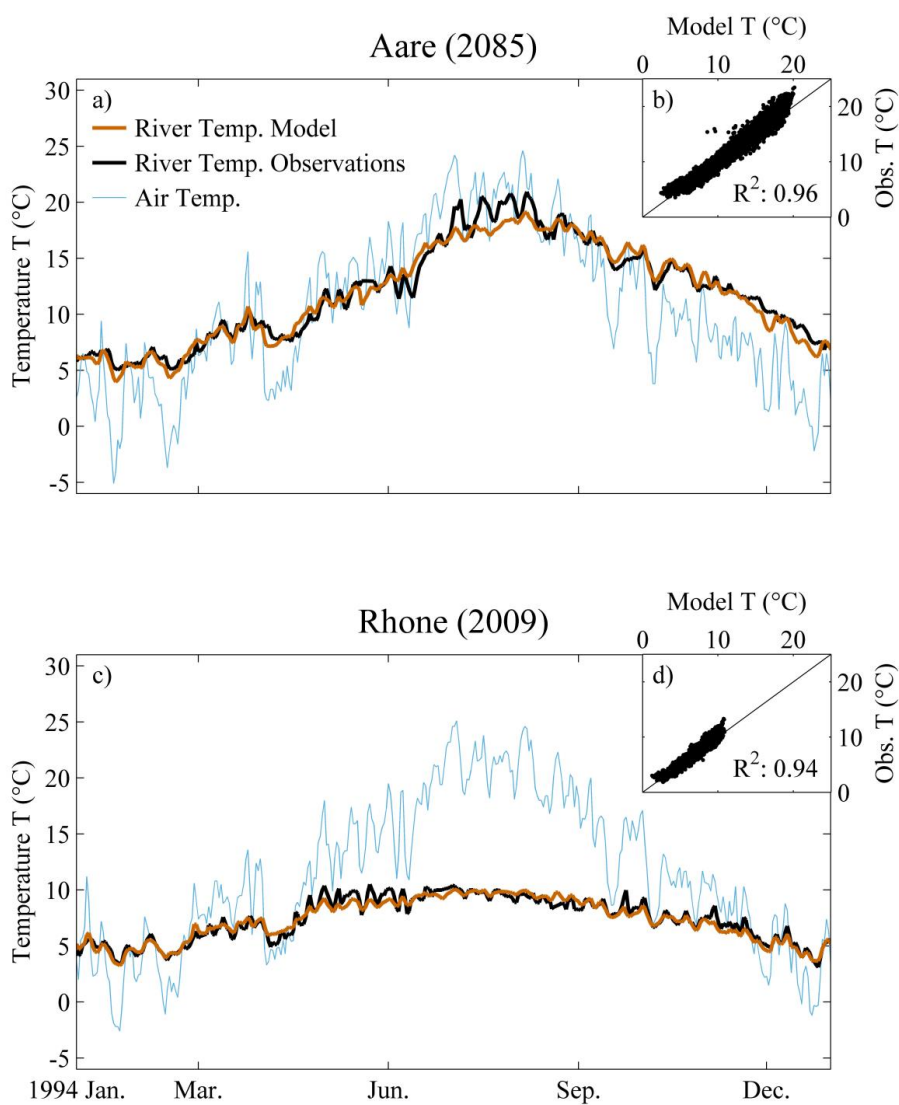
757

758 **Figure 2.** Study area and regional air temperature increases predicted under climate change scenarios addressed
 759 here. Elevation above sea level (green to white color ramp), locations and number of river stations (white
 760 diamonds), drainage area (Aare: vertical lines; Rhône: horizontal lines) and location of Mühleberg Nuclear Power
 761 Plant (MNPP, orange circle). Area covered by regional climate models (dark red dashed-dotted line) with a)



762 predicted air temperature increase ΔT in the near-future (blue, 2030-2049) and far-future (orange, 2080-2099) for
763 medium (thick lines) and upper/lower estimates (thin lines) under the A1B emission scenario (CH2011, 2011).

764



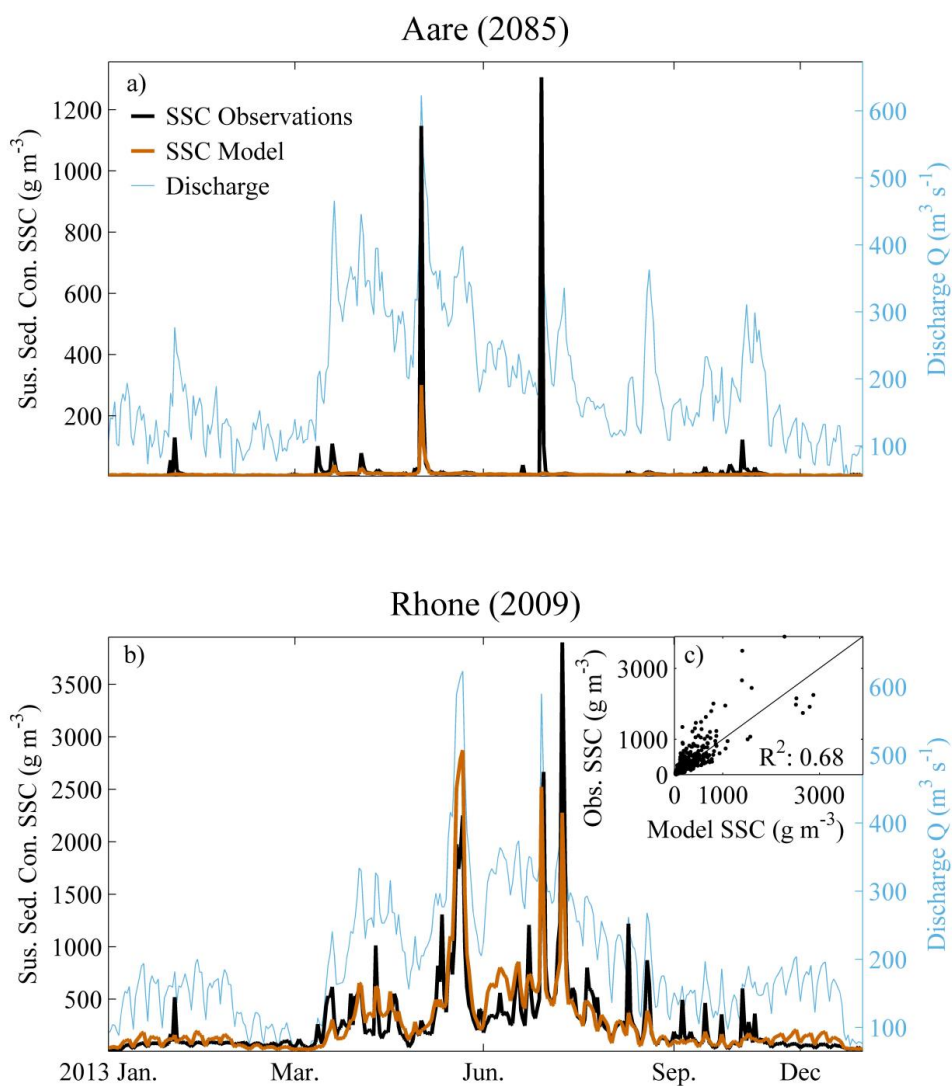
765

766 **Figure 3.** Air2stream modeled (orange) and measured (black) temperature (T) compared to air temperature (blue)
767 for a) Aare River and c) Rhône River in 1994. The insets b) and d) show modeled versus observed temperature
768 from 1990 to 2009 with coefficient of determination (R^2).

769



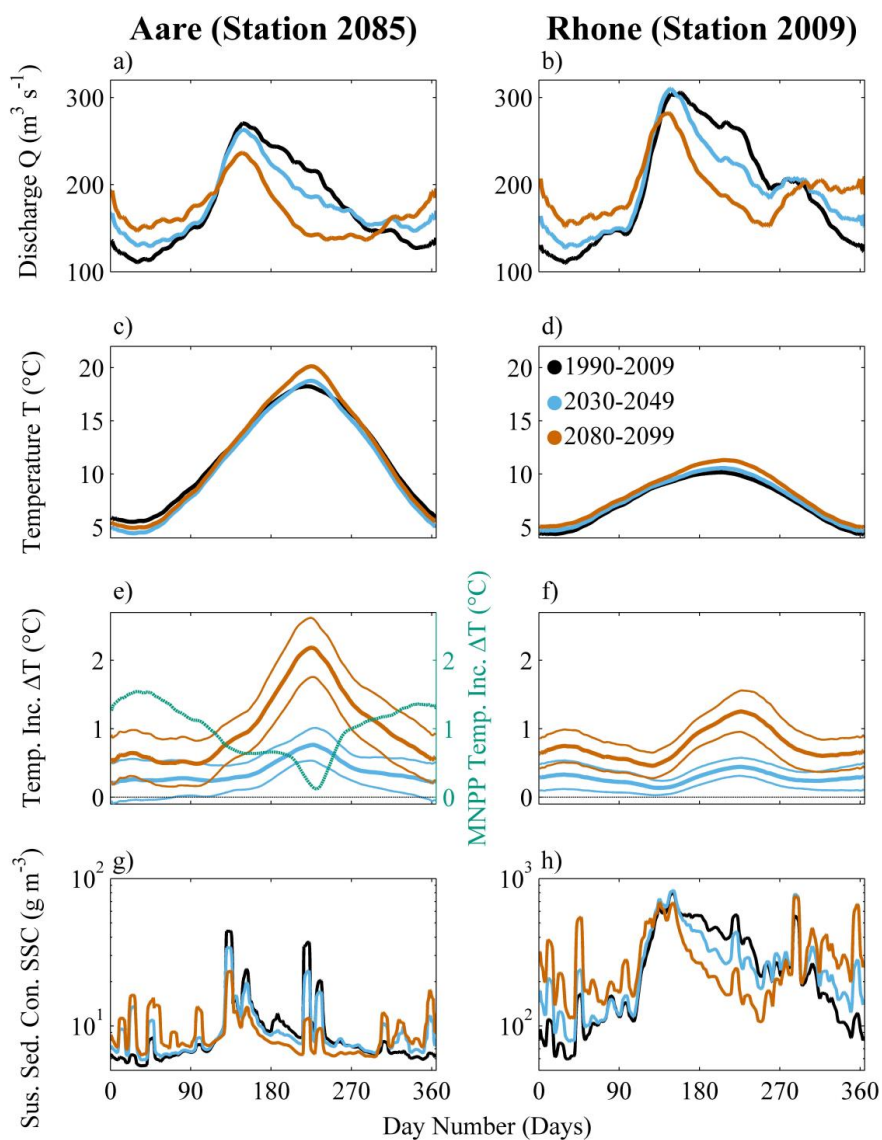
770



771

772 **Figure 4.** Modeled (orange) and measured (black) suspended sediment concentration (SSC) compared to river
773 discharge Q (blue) for a) Aare River and b) Rhône River in 2013. The insets c) shows modeled versus observed
774 SSC for 2013 and 2014 with coefficient of determination (R^2).

775

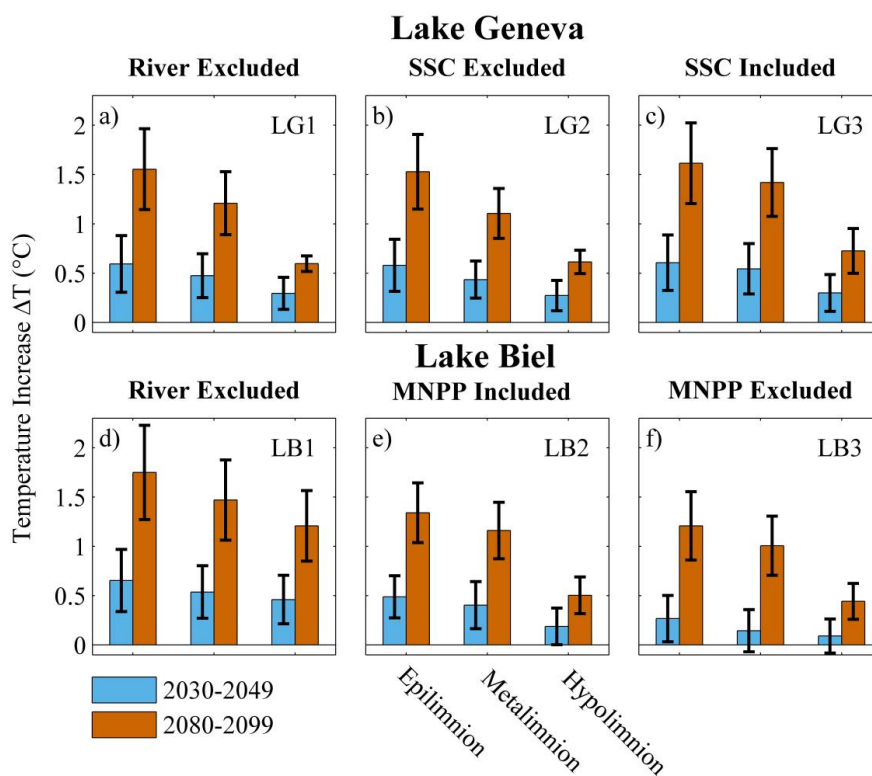


776

777 **Figure 5.** Modeled climate impact from scenarios LB3 (Aare River, left column) and LG3 (Rhône River, right
 778 column) displayed as daily average for reference (black, 1990-2009), near-future (blue, 2030-2049) and far-future
 779 (orange, 2080-2099) time periods. Discharge Q (a and b), net water temperature T (c and d) with anthropogenic
 780 heat from Mühleberg Nuclear Power Plant (MNPP) removed from near-future and far-future time periods,
 781 temperature increase ΔT (e and f) due to climate change (orange/blue) and MNPP (blue-green) as well as modeled
 782 SSC (g and h). Maximum and minimum modeled values are marked by fine lines (e and f) and or are omitted (c,
 783 d, g, and h) for clarity.



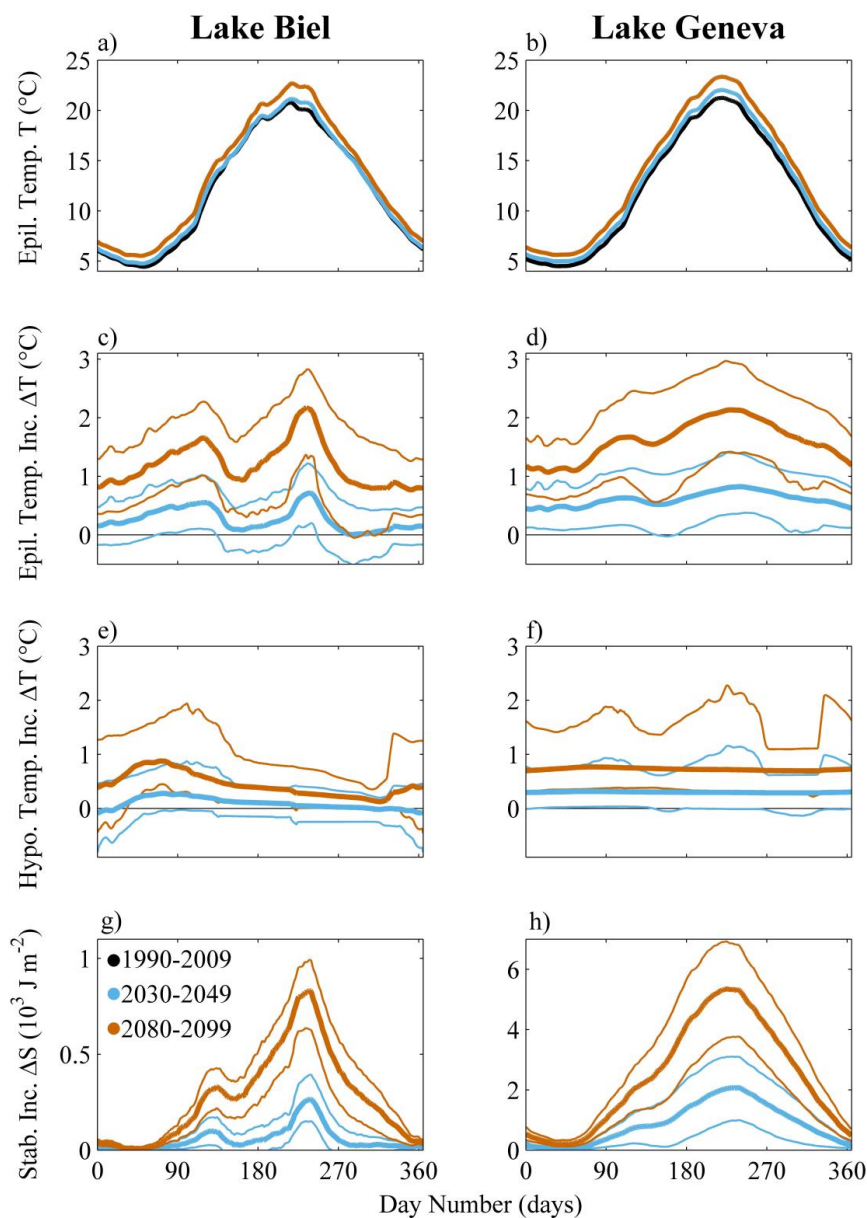
784



785

786 **Figure 6.** Temperature increase ΔT for near-future (blue) and far-future (orange) time periods relative to reference
 787 period temperatures, displayed as mean (bars) and standard deviation (black lines). Epilimnion (left pair of bars),
 788 metalimnion (middle pair) and hypolimnion (right pair) in LG (a to c) and LB (d to f). Graphs represent river
 789 intrusion excluded (a and d), river-borne SSC included (c, e and f) and excluded (b), Mühleberg Nuclear Power
 790 Plant (MNPP) heat release included in (e) and excluded (f) from near-future and far-future time periods but
 791 retained for the reference period.

792



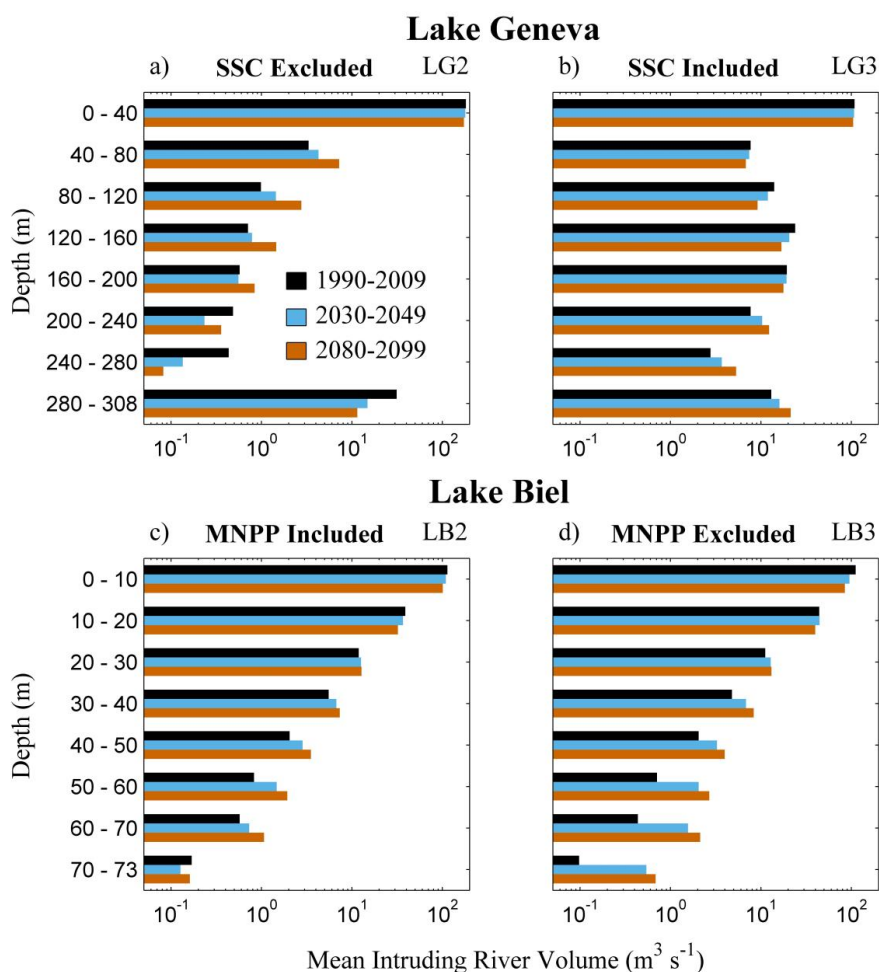
793

794 **Figure 7.** Modeled climate impact from scenarios LB3 (LB, left column) and LG3 (LG, right column) displayed
 795 as daily mean (thick lines) and maximum/minimum model values (thin lines) for near-future (blue, 2030-2049)
 796 and far-future (orange, 2080-2099) time periods relative to the reference period (black, 1990-2009).
 797 Anthropogenic MNPP heat input entering LB has been excluded from near-future and far-future time periods but



798 retained for the reference period. Temperature T (a and b), increase of temperature ΔT in epilimnion (c and d) and
 799 hypolimnion (e and f) as well as increase in stability ΔS (g and h).

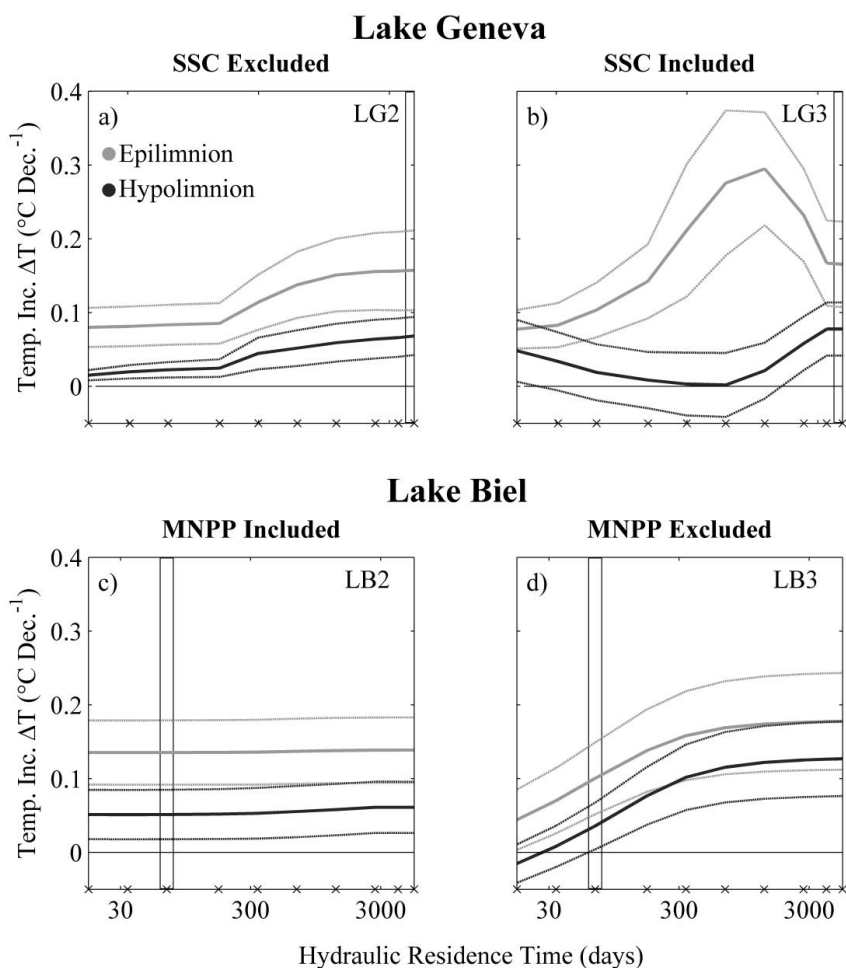
800



801

802 **Figure 8.** Modeled climate impact on mean intruding river volume. Reference (black), near-future (blue) and far-
 803 future (orange) time periods for LG (a to b) and LB (c to d), including (b, c and d) and excluding (a) river borne
 804 SSC and anthropogenic MNPP input included in (c) or excluded from (d) near- and far-future time periods but
 805 retained in the reference period.

806



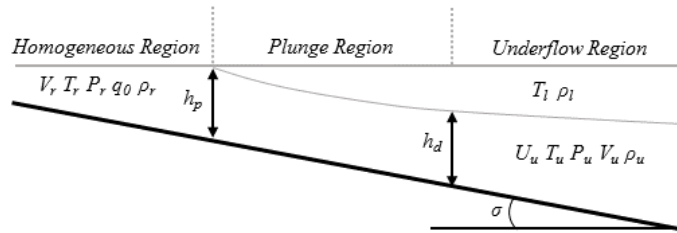
807

808 **Figure 9.** Variation in lake hydraulic residence times (changed lake volume) in response to modeled temperature
 809 increase (ΔT) in the epilimnion (grey) and hypolimnion (black) displayed as decadal mean (solid line) and
 810 standard deviation (dotted line) for LG (a and b) and LB (c to f). River borne SSC included (b) and excluded (a,
 811 c and d), MNPP heat input included in (c) and excluded from (d) near-future and far-future time periods but
 812 retained for the reference period. Black x's mark observed lake residence times and black rectangles mark the
 813 unmodified residence times.

814



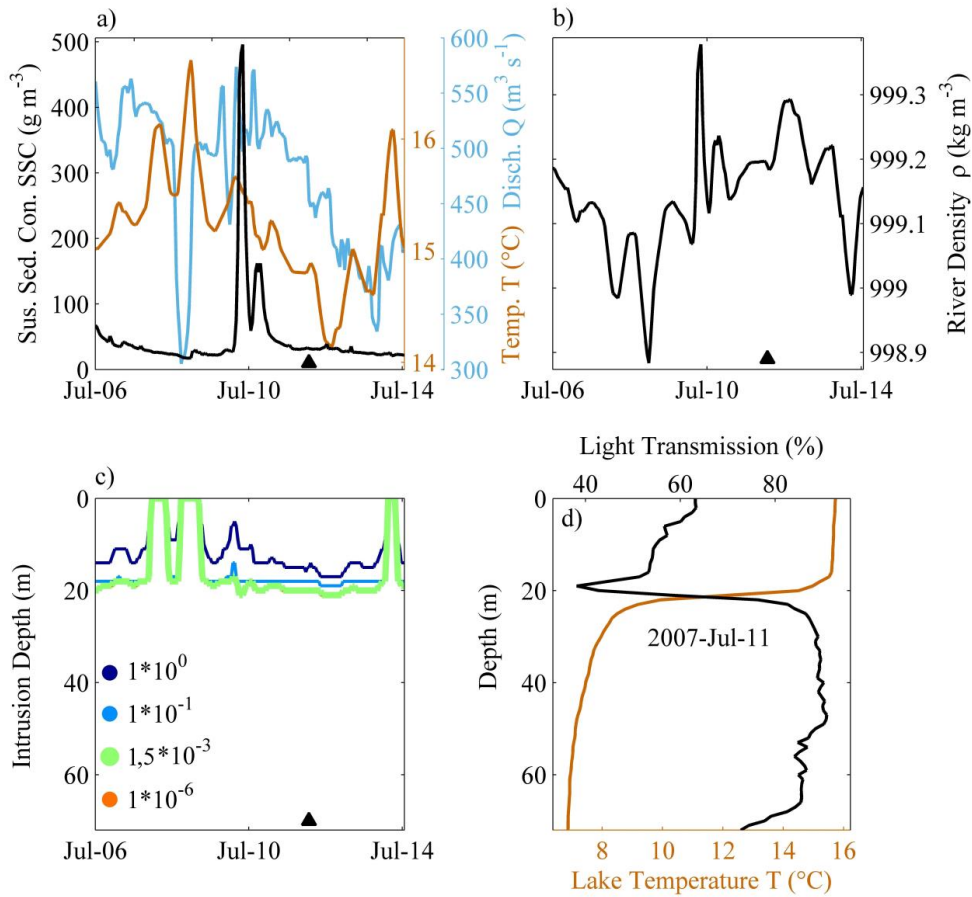
815 **Appendix Figures**



816

817 **Figure A1.** Illustration of river intrusion model.

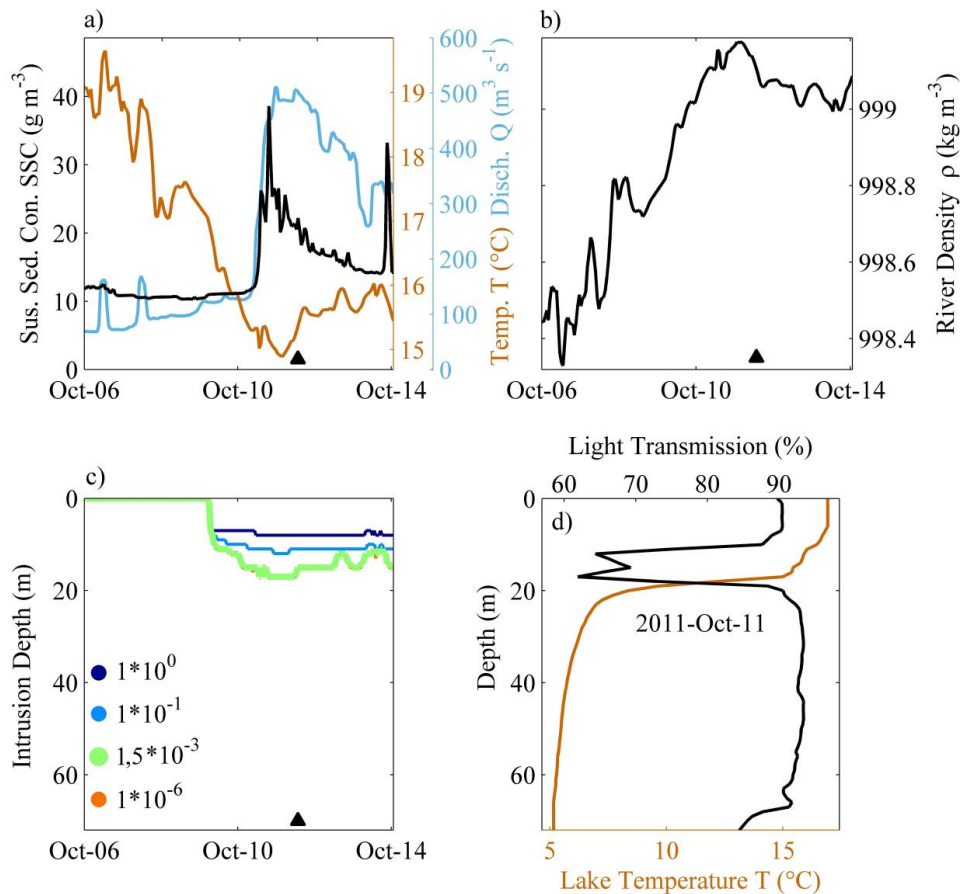
818



819



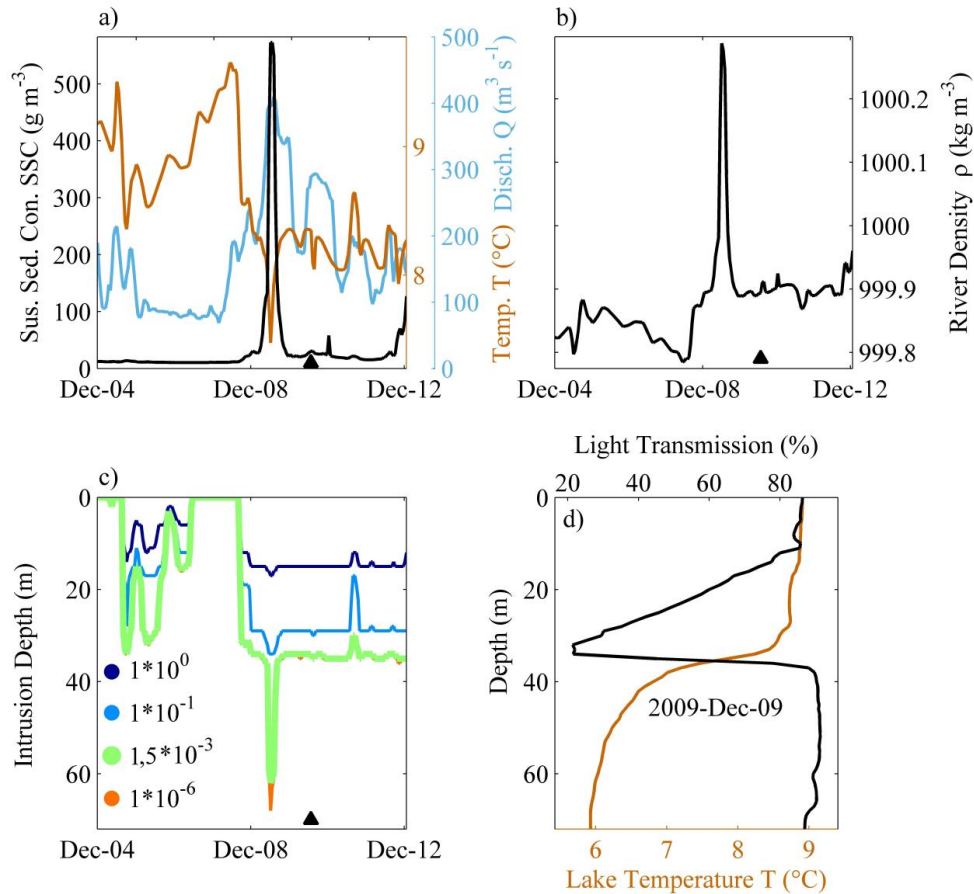
820 **Figure A2.** River intrusion entrainment sensitivity analysis for the LB/Aare system in July 2007. a) SSC (black),
 821 temperature (T; orange) and river discharge (Q; blue) from Aare station 2085. b) River density at station 2085
 822 obtained from T and SSC in a). c) River intrusion depth calculated from supporting information (S1) with varying
 823 entrainment constant β (Eq. 18); light green denotes the value used in this study. d) Vertical measurements of T
 824 and light transmission in LB for 11th July 2007. \blacktriangle marks the time in a) to c) of the vertical profile in d).
 825



826
 827 **Figure A3.** River intrusion entrainment sensitivity analysis for the LB/Aare system in October 2011. a) SSC
 828 (black), temperature (T; orange) and river discharge (Q; blue) from Aare station 2085. b) River density at station
 829 2085 obtained from T and SSC in a). c) River intrusion depth calculated from supporting information (S1) with
 830 varying entrainment constant β (Eq. 18); Light green denotes the value used in this study. d) Vertical
 831 measurements of T and light transmission in LB for 11th October 2011. \blacktriangle marks the time in a) to c) of vertical
 832 profile in d).



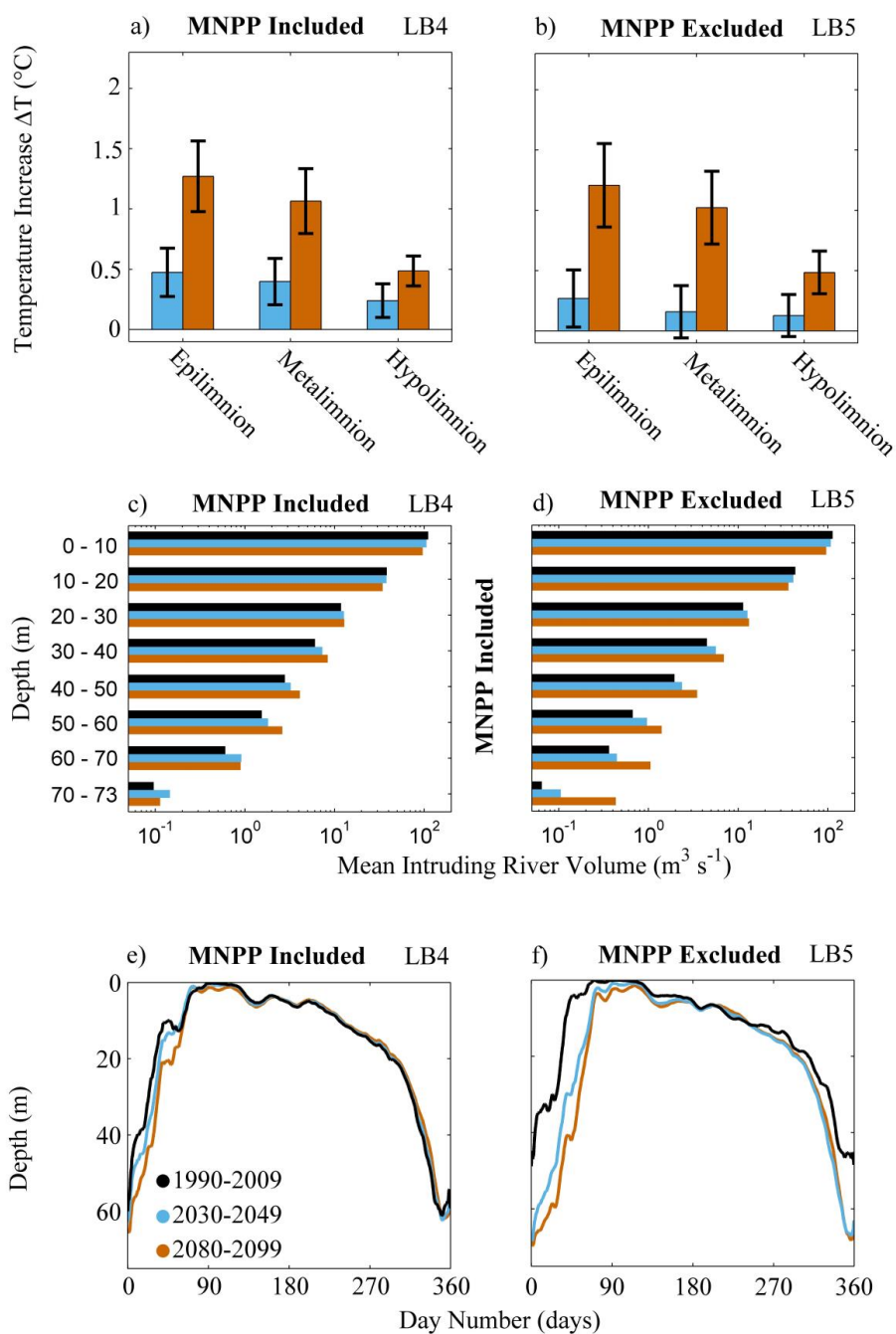
833



834

835 **Figure A4.** River intrusion entrainment sensitivity analysis for the LB/Aare system in December 2009. a) SSC
 836 (black), temperature (T; orange) and river discharge (Q; blue) from Aare station 2085. b) River density at station
 837 2085 obtained from T and SSC in a). c) River intrusion depth calculated from supporting information (S1) with
 838 varying entrainment constant β (Eq. 18); light green denotes the value used in this study. d) Vertical measurements
 839 of T and light transmission in LB for 9th December 2009. ▲ marks the time in a) to c) of vertical profile in d).

840



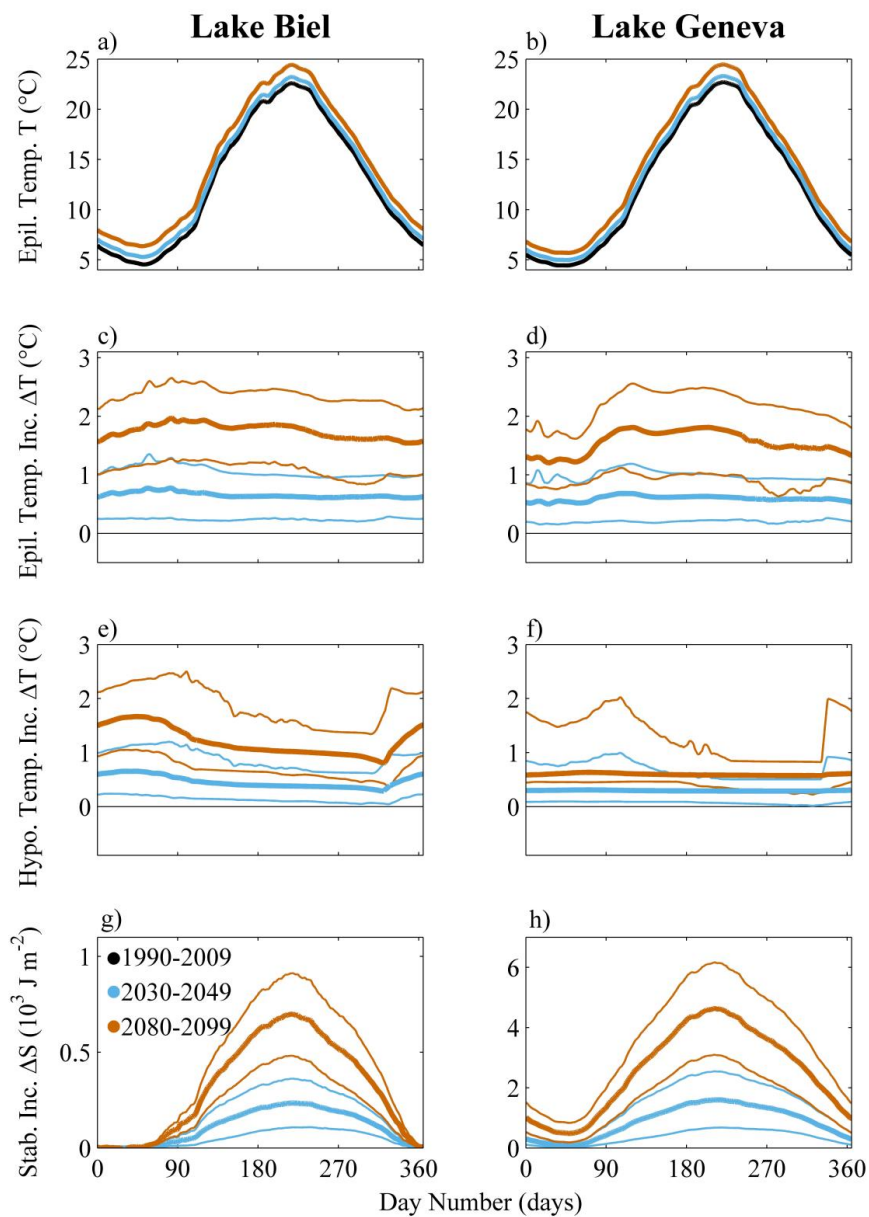
841

842 **Figure B1.** Modeled climate impact on LB excluding river borne SSC. Temperature increase ΔT (a and b)
 843 displayed as means (bars) and standard deviations (black lines) in epilimnion (left bar group), metalimnion
 844 (middle bar group) and hypolimnion (right bar group); mean intruding river volume (c and d) and mean river



845 intrusion depth (e and f). MNPP thermal input included (a, c and e) or excluded (b, d and f) in near-future (blue)
 846 and far-future (vermillion) time periods but retained in the reference period (black).

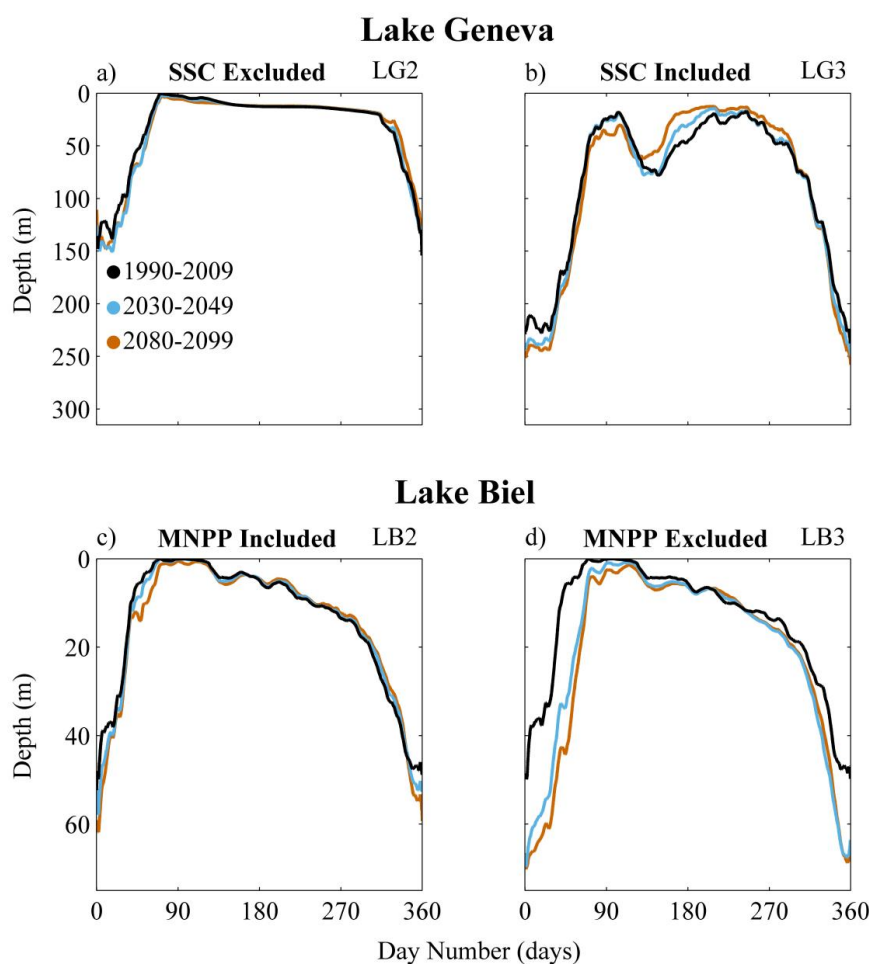
847



848



849 **Figure C1.** Modeled climate impact (river intrusion excluded) on LB (left column, scenario LB1) and LG (right
850 column, scenario LG1) shown as daily mean (thick lines) and maximum/minimum model values (thin lines) for
851 near-future (blue, 2030-2049) and far-future (orange, 2080-2099) time periods relative to the reference period
852 (black, 1990-2009). Temperature T (a and b), temperature increase (ΔT) in the epilimnion (c and d) and
853 hypolimnion (e and f) as well as increase in stability (ΔS ; g and h).
854



855

856 **Figure D1.** Modeled climate impact on mean river intrusion depth. Reference period (black), near-future (blue)
857 and far-future (orange) time periods for LG (a to b) and LB (c to d) with (b, c and d) and without (a) river borne
858 SSC and MNPP thermal input included (c) or excluded (d) from near-future and far-future time periods relative
859 to the reference period.

860